1 General

Aluminum Alloy A357.0 is a premium Mg_2Si casting alloy developed for applications in the aerospace industry. It is normally produced to a standard specification as A357.0 and to a more carefully controlled specification as D357.0. The latter variety requires control of the dendrite arm spacing (DAS), tighter composition limits on impurities, radiographic requirements and in some cases requirements on fracture toughness and fatigue properties. Mechanical properties of F_{tu} = 50 ksi, F_{ty} = 40 ksi, and e = 5 percent can be obtained in properly engineered castings of this alloy. Large complex castings having thin and thick intersecting sections have been produced from A357.0 and D357.0. These castings have passed the same qualification tests applied to similar built-up wrought aluminum structures. Such cast parts, if put into production, can be cost efficient as compared to similar built-up wrought parts. It should be emphasized that castings for critical applications should be produced by foundries qualified for the production of premium castings. The important features for such qualification and the expected performance have been established by several Air Force programs that form the principal basis for this section.

It should be noted that the AMS Specifications for D357.0 were written after the major Air Force Programs were completed and, strictly speaking, it is not possible to directly connect the data in this section with these new Specifications. However, where the composition and mechanical properties conform to the AMS Specification for D357.0, the data are designated as D357.0; otherwise the data are designated as A357.0.

1.1 Commercial Designations

Cast A357.0, Cast D357.0

1.2 Alternate Designations - See Table 1.4.2

1.3 Specifications

AMS 4219C, AMS 4249, AMS 4241A, AMS 4246B, MIL-A-21180D, and ASTM B 108.

1.4 Composition

1.4.1 General. Magnesium and silicon are the major alloying elements with Mg_2Si being the primary hardening agent during aging. Tensile strength increases and ductility decreases with increasing amounts of magnesium, as shown in Figure 1.4.3.1. However, increases in magnesium content above about 0.6 percent have little effect on the tensile properties. The only other elements intentionally added are beryllium and titanium. They do not contribute significantly to the strength but have indirect beneficial effects. Thus, beryllium tends to reduce the oxidation of magnesium during melting, and to scavenge iron, which tends to form a brittle, intermetallic, Fe-Si phase that reduces ductility. Titanium is a grain refiner providing a fine dispersion of TiAl particles in the melt which act as nuclei for the primary aluminum dendrites. As will be discussed later, attempts are often made to control the eutectic microstructure through the additions of modifiers such as sodium or strontium. (See 1.8.5)

	Al
7.0	Si
0.6	Mg
0.15	Ti
0.05	Be

1.4.2 *[Table]* AMS and ASTM composition for A357.0 and D357.0.

1.4.3 Effect of element contents on tensile properties.

1.4.3.1 *[Figure]* Effect of magnesium content on the tensile properties of shell investment castings.

1.4.3.2 *[Figure]* Effects of iron, beryllium, and magnesium contents on tensile and fracture properties of plates cast in permanent molds.

Beryllium offsets to some extent the negative effects of increasing iron content.

1.4.3.3 *[Table]* Average tensile, notch yield strength ratio, and percent porosity for specimens cut from cast blocks produced with two chill rates and aged at two temperatures.

The faster Cu chill resulted in higher elongation, somewhat higher NTS/F_{ty} ratio, and less porosity. Age treatment significantly affected only the NTS/F_{ty} ratio for the slower Fe chill.

1.4.3.4 *[Figure]* Relative effects of silicon content on tensile properties of D357.0-T6 sand-castings.

Increasing Si content significantly decreases elongation, while causing only minor relative reduction in other tensile properties.

1.4.3.5 *[Figure]* Relative effects of magnesium content on tensile properties of D357.0-T6 sand-castings.

Within the specification range, increasing Mg content reduces elongation, but has little relative effect on other tensile properties.

1.4.3.6 *[Figure]* Relative effects of the combined titanium, manganese, and beryllium contents on tensile properties of D357.0-T6 sand-castings.

Increasing the content of these three elements reduces elongation and has little relative effect on other tensile properties.

This section produced with the support of NASA-Lewis Research Center.

1.5 Heat Treatment

1.5.1 The heat treatment for both A357.0 and D357.0 is given in the applicable AMS specifications as 1000F to 1020F solution treatment with the solution time, quenching media and aging temperature being selected to produce the specified properties. The following heat treatment may be used as a guide: Solution treat 1000F to 1020F, 12 to 15 hours, followed by quenching in water with 15 percent ethylene glycol, and aging at 315 to 325F for 4 to 12 hours to produce the T6 condition. Quench delay time does not appear to be important.

Attempts to improve the properties of A357.0 by hot isostatic pressing of the as-poured castings were not successful. The cooling rates from the isostatic press are so slow that the alloy had to be solution heat treated following pressing. The process was able to close porosity but was not able to produce significant improvement over that obtained by the best normal foundry practice without hot isostatic pressing. (Ref. 25)

1.5.2 While the tensile properties decrease with increasing quench-water temperature (see Figure 1.5.6), a cold-water quench increases residual stress gradients and distortion in thin sections. These problems are minimized by quenching in warm water [e.g., 160F (Ref. 10)] or by the use of a water + glycol quench. Generally, the water is at room temperature and 15 to 25 percent ethylene glycol is added. It is common practice to delay aging for 16 hours following quenching. This delay tends to increase the elongation with only a slight decrease in tensile strength (Ref. 30). This effect may be inferred from Figure 1.5.9.

1.5.3 Straightening must be performed in the solution-treated condition.

1.5.4 *[Figure]* Effect of solution-treatment time on tensile properties of shell investment castings.

1.5.5 *[Figure]* Effect of solution-treatment time on tensile properties of sand-castings.

1.5.6 *[Figure]* Effect of quench-water temperature on tensile properties of shell investment castings.

1.5.7 *[Figure]* Effect of quench-water temperature on tensile properties of sand-castings.

1.5.8 *[Figure]* Effect of delay time between solution treatment and quench for shell investment castings.

1.5.9 *[Figure]* Effect of delay time between solution treatment and quench for sand-castings.

1.5.10 *[Figure]* Effect of aging time on tensile properties of investment castings.

1.5.11 *[Figure]* Effect of aging time on tensile properties of sand-castings.

1.6 Hardness

(See Figures 2.2.2.1, 2.2.2.2 and Table 3.1.1)

1.7 Forms and Conditions Available

Castings

1.8 Melting and Casting Practice

1.8.1 General. The mechanical properties of a casting are complex functions of the melting and pouring techniques, mold and core making, chilling and insulation, and the gating and risering methods. There are no general rules which may be applied to all types of castings and for critical applications a carefully planned development phase is essential. During a period from 1977 to 1984 the Air Force sponsored development programs at Northrop, General Dynamics, and Boeing. The goal of these programs was to develop cost-effective manufacturing methods and design specifications for the production of large, complex castings suitable for use in high-performance aircraft. The alloy A357.0-T6 was featured in these programs. The program at Northrop was concentrated on establishing an optimum composition for a premium A357.0 casting alloy (later designated as D357.0) and the development of design mechanical properties. The General Dynamics program demonstrated the successful production of an F-16 vertical-tail understructure. The Boeing "CAST" program was concerned with details of the casting process and the production of a large, thin-walled casting for the nose gear support bulkhead for the YC-14 airplane. The summary of foundry practices in Sections 1.8.3 and 1.8.4 is primarily taken from this program.

For assessment of mechanical properties, the following types of castings were used:

Northrop - Shell investment and composite, sand-cast, uniform-thickness plates (Tables 3.2.1.4 and 3.2.1.5) and stepped-plate, composite sand-castings with a designated area representing the maximum thickness which could be examined to insure detection of Grade B soundness (Figure 1.8.1.1).

General Dynamics - Separately cast sections of the vertical-tail understructure for the F-16 (Table 3.2.1.6) and the full casting (Table 3.2.1.7).

Boeing - Separately cast sections of the full-scale bulkhead shown in Figures 1.8.1.2 and 1.8.1.3.

1.8.1.1 *[Figure]* Sand-mold, stepped-plate configuration used in the Northrop Program to determine design property data for sand-cast A357.0-T6 from two suppliers. A (Magnesium Alloy Products) and B (Teledyne Cast Products). Two integral tensile coupons attached to optional locations.

1.8.1.2 *[Figure]* Large, thin-walled, composite sand-cast nose-gear support bulkhead for the YC-14 airplane. Ten identical castings were each produced by the Boeing and the Hitchcock Foundries using Boeing-developed manufacturing plans and tooling.

1.8.1.3 *[Figure]* Nose landing-gear support bulkhead casting showing locations of specimens removed from five sections of the casting (each section heat treated separately).

1.8.2 Fluidity. Good fluidity is especially important in the production of complex, thin-walled castings in order to avoid cold shuts and shrinkage defects. The double spiral fluidity test (Figure 1.8.2.1) was used to evaluate the effects of mold, sand, mold coatings, and alloy composition (Ref. 10). AFS 53, 70, and 140 silica sands were investigated with a sodium silicate - CO_2 binder. In addition, tests were made using zircon and chromite sand. Best results were obtained with AFS 70 sand. The effects of amorphous carbon and hexachlorethane mold coatings were investigated with the configuration shown in Figure 1.8.2.1, using AFS 70 mold sand and a pouring temperature of 1400F. The best results were obtained with amorphous carbon, which produced a 40 percent increase in fluidity compared with uncoated molds. Variations of silicon, magnesium, and beryllium within the composition limits of the alloy did not affect the fluidity.

1.8.2.1 *[Figure]* Double spiral fluidity test casting.

1.8.3 Holding temperature. The charge of molten metal is held until degassing and mold preparation are complete. Holding temperatures from 1250 to 1450F were investigated for holding times from essentially 0 to 24 hours. Charges were melted in 350-pound-capacity, silicon carbide crucibles with a minimum amount of surface exposed to the atmosphere (Ref. 5). Results showed that neither temperature nor holding time within the ranges investigated had a significant effect on silicon, magnesium, or beryllium contents of the melt, but that the amount of hydrogen in the melt increased with holding temperature and slightly with holding time. Based on these results, the holding temperature prior to degassing is suggested to be in the range between 1250 and 1325F.

1.8.4 Degassing. Hydrogen is the only gas having measurable solubility in aluminum. As shown in Figure 1.8.4.1, the solubility decreases rapidly as the melt cools to the solid state. This decrease in solubility results in trapped hydrogen gas in the form of porosity in the casting. The source of hydrogen is the reaction between molten aluminum and water. Water may be introduced into the melt in various ways including the products of fuel combustion, mold coatings, moisture absorbed or chemically combined with fluxes (the reaction products of fluxing with chlorine are highly hygroscopic), moisture adsorbed on the surface of the charge components or tools and moisture in the air.

The amount of hydrogen in the melt can be determined accurately by use of the Telegas analyzer (Ref. 11). This instrument is not generally suitable for use in a production environment and a so-called "vacuum-freeze" test is widely used. In this test a small sample of the melt is slowly solidified under a vacuum of about 5 mm of Hg, and watched carefully for the appearance of bubbles. Bubble formation is strongly resisted by the surface tension of the melt, but is greatly enhanced by the presence of minute inclusions. The presence of inclusions complicates the interpretation of the vacuum freeze test as an indicator of hydrogen content. However, the absence of bubbles coupled with the absence of porosity in the sectioned sample does indicate low hydrogen content. Boeing recommended that the hydrogen content of A357.0 not exceed 0.15 ml/100 gm within 2 hours of pouring (Ref. 10).

Boeing investigated three methods of degassing, namely the introduction of nitrogen gas, hexachlorethane, and a gaseous mixture of 90 to 95 percent nitrogen plus 10 percent chlorine. Degassing temperatures ranged from 1250 to 1400F, with times up to 2 hours. Satisfactory results were obtained (Figure 1.8.4.2) using either nitrogen with a carefully controlled flow rate or with a mixture of nitrogen and chlorine gas, with this mixture providing the most rapid degasification. Hexachlorethane was added in the form of tablets at a melt temperature of 1300 to 1350F. This chemical reacts with aluminum to produce a bubbling reaction. The effect of 2- to 4-ounce additions to a 350-pound melt was found to be unsatisfactory in that an increase in hydrogen content was observed (Ref. 5). The effect of a dried NaCl/KCl overflux was evaluated for the prevention of hydrogen absorption and removal of oxides. The hydrogen content increased due to the hygroscopic nature of the flux. Boeing points out that when using chlorine as a degassing agent, all degassing tools should be preheated prior to immersion in the melt. Omission of this precaution may result in an explosion. Degassing with the nitrogen-plus-chlorine mixture at 1250 and 1300F did not produce a loss of alloy constituents but at 1400F there was a loss of magnesium and beryllium.

1.8.4.1 *[Figure]* Solubility of hydrogen in solid and molten aluminum as a function of temperature.

1.8.4.2 *[Figure]* Effect of degassing time and temperature on hydrogen content.

1.8.5 Eutectic modifiers. The interdendritic phases consist primarily of silicon and the binary eutectic, Al + Si, which together constitute about 90 percent of the interdendritic particle area. Other interdendritic phases include the ternary eutectic (Al + Si + Mg_2Si) and complex compounds of Al-Fe-Si-X (Ref. 21). Ideally, the interdendritic structure should be finely divided and spheriodal. Acicular forms tend to reduce the alloy ductility. The interdendritic morphology is controlled in part by the phosphorus content with acicular silicon particles being associated with increasing phosphorus (Ref. 27). The phosphorus may be

effectively removed by the addition of sodium or strontium. These elements form compounds with magnesium, and these compounds combine with the phosphorus. The result is a fibrous eutectic. However, the use of these modifiers is not without problems. Sodium has a much higher reactivity than strontium at molten aluminum temperatures and tends to burn off. Boeing (Ref. 5) found that the addition of sodium tended to produce bubbles and increased the hydrogen content. Degassing following the introduction of sodium reduced the sodium level below that required for eutectic modification.

The addition of strontium did not produce a visible reaction, but the melt hydrogen content increased and degassing depleted the strontium content. Considering the problems associated with sodium and strontium additions, Boeing chose not to use modifiers but depended on controlled solidification rates to produce a satisfactory microstructure. However, strontium is a frequently used modifier and antimony also has been used (Ref. 26). It has the advantage of being unaffected by holding time, degassing, or remelting. However, it produces a lamellar eutectic microstructure which is somewhat inferior to the fibrous type.

1.8.5.1 *[Figure]* Effect of strontium content on the ratio of notched tensile strength to tensile yield strength of D357.0-T6 sand-castings.

1.8.6 Pouring temperature. Pouring temperature for large thin-walled castings is very critical. If the temperature is too high, a coarse grain structure will result along with porosity, shrinkage, and oxide formation. If the temperature is too low, misruns, cold shuts, and shrinkage can be encountered. The pouring temperature for aluminum castings is usually between 1325 and 1450F. In the Boeing program, pouring temperature was investigated over the range from 1350 to 1450F using the test-plate configuration shown in Figure 1.8.6.1. The highest values of F_{tu}, F_{ty}, and e were obtained for those specimens nearest the chill, and poured at 1350F.

1.8.6.1 *[Figure]* Test plate configuration incorporating a chill.

1.8.7 Mold and core making. In general, molds and cores should be strong enough to permit handling and to resist deterioration by the molten metal, have good permeability to evolved gases, hold dimensional tolerances, and provide good shake-out capability. Sand types and binder combinations were investigated in the Boeing program (Ref. 5). Round-grain silica sands were found to be superior to the angular, olivine types in terms of flowability during molding and in terms of casting surface finish. AFS 70 silica sand was compared with olivine sand using a synthetic resin binder. Results showed a pronounced superiority for the silica sand in terms of tensile and compressive strength as a function of storage time and in terms of permeability. In addition to the synthetic resin binder, similar tests were also conducted with silica sand using sodium silicate cured with CO_2, sodium silicate no-bake, and oil-urethane no-bake systems. While silica sand bonded with sodium silicate systems displayed good mold properties, the strengths obtained decreased after relatively short (20 hours) storage time. Poorest performance was obtained using the synthetic resin binders. On balance, the best performance in terms of strength after prolonged storage, was obtained with no-bake, oil-urethane binders (e.g., Linocure). However, the bonding reaction of this system is extremely temperature sensitive and sand temperature must be above 65F.

1.8.8 Parting agents. Parting agents are used to prevent the mold sand from sticking to the pattern or the mold section interfaces. Parting agents are often recommended by the manufacturer of the binders. In the Boeing program, all parting agents were spray or brush applied. With the Linocure binder system, Ashland L 16 provided fine detail pickup and was otherwise satisfactory. (Ref. 5)

1.8.9 Mold leveling. When using molds with multiple flasks for large castings, leveling can be critical. Boeing (Ref. 5) found that for castings such as shown in Figure 1.8.1.2, leveling with a telescope was far more accurate than using a bubble level.

1.8.10 Insulation materials. Materials such as plaster, ceramic, and fibrous material are commonly used to insulate risers and in some cases thin sections to improve the fluidity of the molten metal in order to avoid cold shuts or misruns. Typically, aluminum castings will display a decrease in volume of about 6.5 percent during solidification. This shrinkage is controlled by proper placement of insulated risers. Investigations during the Boeing program (Ref. 5) showed that plaster, even when followed by long drying, outgassed when contacted by molten metal. The optimum material for riser insulation appeared to be a paper-fiber-glass composite, and for insulation of thin sections, a ceramic-foam block.

1.8.11 Chill size and location. The purpose of chills in a mold is to promote directional solidification and a desirable microstructure. In the Boeing program (Ref. 5), chill materials were investigated using the configuration shown in Figure 1.8.6.1. Iron, aluminum, copper, and graphite were compared in their effects on tensile properties for specimens taken 1, 4, 8, and 11 inches from the chilled end. Chill size and shape were also investigated using aluminum. Substantial increases in tensile strength and elongation were obtained using any of the chill materials, as compared with values obtained without a chill (e.g., Figure 1.8.11.1). As might be expected, the largest increase in properties occurred nearest the chilled end. For a given volume of chill material, copper produced the highest tensile strength and elongation. Chill shape for equal volume did not exhibit a significant effect. The tensile yield strength was little affected by the presence of chills. The results indicated that the mass of the chill should be equal to

one to two times the mass of the metal being chilled. Copper chills are expensive, and a combination of copper and aluminum chills can be used to reduce costs. Copper chills might be used in sections greater than 1-inch thick, while aluminum chills could be used in lighter sections. The location and size of chills will, of course, depend on the casting configuration. In large thin-walled castings which incorporate complex gating systems and numerous risers, chills must be used extensively to control proper metal solidification.

1.8.11.1 *[Figure]* Effect of various chill metals and distance from the chill for sand-castings (derived from Ref. 5, Figures 55, 56).

1.8.11.2 *[Figure]* Configuration of fatigue test specimen used to measure the effects of chill rates and aging processes on high-cycle fatigue life.

1.8.11.3 *[Figure]* Effect of chill rates and aging processes on tension-tension fatigue life of notched specimens of D357.0 alloy at 20 ksi maximum stress.

Little effect of aging process was found, but the faster solidification rate with Cu chills almost doubled average fatigue life, compared to the slower solidification rate with Fe chills. This improvement appears to be at least partially the result of lower porosity with the faster solidification, as noted on the figure.

1.8.11.4 *[Figure]* Effect of porosity resulting from different chill rates and aging processes on tension-tension fatigue life of notched specimens of D357.0 alloy at 20 ksi maximum stress.

Porosity alone has a minor effect on fatigue life at levels below 0.04 percent. Above 0.04 percent, average fatigue life decreases significantly with increasing porosity

1.8.11.5 *[Figure]* Effect of magnesium content on tension-tension fatigue life of notched specimens of D357.0 alloy at 20 ksi maximum stress, with different chill rates and aging processes.

Increasing Mg content from 0.45 to 0.55 percent dramatically increases fatigue life when coupled with faster solidification rates. At the slower solidification rate some fatigue life increase is also seen. These results confirm the expected strengthening benefits of additional eutectic.

1.8.12 Gating and risering. Boeing (Ref. 5) used complex, thin-walled castings of several designs to investigate optimum gating and risering techniques. Horizontal gating is most commonly used because it produces low metal turbulence, but large thin-walled castings present problems of nonuniform directional solidification and mold sag if cast in the horizontal position. When castings are made in the vertical position, directional solidification is enhanced because metal is gated into the casting only when it is required to fill space. Solidification is then controlled by proper use of chills. In contrast, horizontal castings are usually filled from the bottom of the mold cavity and then into the risers, with the result that all metal must pass through the casting before solidification can begin. This gives rise to nonuniform directional solidification and associated reduced mechanical properties. The disadvantage of a vertical gating system is a large sprue height, which if not properly accounted for in the sprue design can give rise to turbulence.

An unpressurized gating system should be employed where the cross section of the sprue base is less than the sum of the total areas of the runner and ingates. Such a system produces slow, non-turbulent metal flow. Using a metal flow rate of 7 pounds per second, Boeing investigated various gating ratios and concluded that, for large thin-walled vertical castings, a ratio of 1:6:8 should be used where the numbers represent the gross area of sprue, downrunner, and ingate, respectively. As shown in Figure 1.8.12.1, a cascading sprue was used to take advantage of maintaining hydrostatic head with minimum turbulence. To ensure adequate filling in the cascade system, the base area of the upper sprues should be approximately 50 percent greater than lower sprues. All sprues should be tapered to prevent entrapment of air. While conical shape is generally used, Boeing (Ref. 5) found that metal turbulence was reduced by a tapered rectangular design.

Basic features of the pouring well, runner, and ingate are shown in Figure 1.8.12.2. The pouring well is located under the base of the sprue and has as its purpose reduction in the flowing metal velocity. The optimum shape of the well was found to be cylindrical with a flat bottom. Runners should have a square cross section in order to minimize the metal surface area exposed to its walls. There should be a generous radius at the transition from the runner to the ingate in order to reduce turbulence. Ingates should be at the top of the runner so that molten metal fills the runner before it enters the mold and any dross that has formed will rise to the surface and adhere to the sand.

Risers must be designed to permit the solidifying metal to be fed continuously by a reservoir of molten metal from the risers. For thin-walled castings, a large number of closely spaced risers are necessary. The distance from the riser to a chill will influence the mechanical properties, with short distances being desired to increase solidification rates.

1.8.12.1 *[Figure]* Cascading sprue designed to combine good hydrostatic head with minimum turbulence.

1.8.12.2 *[Figure]* Basic features of pouring well, runner, and ingate.

1.8.13 A series of casting trials at a given foundry is typically required to optimize composition, heat treatment, and casting parameters before the required properties of premium castings are obtained. In a research study

conducted by the Aluminum Division Research Committee 2C of the American Foundrymen's Society (Ref. 40), a first set of castings failed to meet strength goals, but was followed by a second set in which yield strength, for example, increased by 30 percent.

1.8.13.1 *[Figure]* Improvement in tensile yield strength from the first to the second set of sand-castings.

1.9 Special Considerations (See also Section 1.8)

1.9.1 Effect of dendrite refinement. The mechanical properties of Al-Si-Mg alloys as well as many other casting alloys are influenced by the dendrite cell size or by a related and, recently, a more widely used measurement, the secondary dendrite arm spacing (DAS). The logarithm of DAS has been shown to be a linearly increasing function of the logarithm of solidification time for a variety of casting alloys (Ref. 22). The smaller the DAS the higher the F_{tu} and the elongation (Ref. 23). This points to the importance of using properly designed chills in the casting of critical parts. The value of F_{ty} is essentially unaffected by DAS. A correlation between DAS and the tensile properties of cast A357.0 is relatively easy to establish for simple cast shapes by examination of the microstructure in a region near the fracture of extracted tensile coupons. Some examples are shown in Figures 1.9.1.1 and 1.9.1.2 for specimens taken from shell investment or composite sand-cast blocks. Two methods of measuring DAS are described in DAE ARP 1947 (Ref. 33): a preferred method, and an alternate method yielding a particle intercept distance (PID) which is less accurate. A surface replication technique for DAS determinations on a cast part has been described (Ref. 29) and is incorporated in the DAS ARP.

If a linear relation is assumed between the DAS and F_{tu} it is possible to specify a maximum DAS value for a casting by determination of the DAS and F_{tu} from two attached tensile coupons having a minimum difference in DAS of 0.001 inch (Ref. 33). Presumably the procedure will ensure that the portion of the casting examined will meet some minimum value of F_{tu}. However, the relationship between DAS and the tensile properties is apparently difficult to determine. In some cases, a linear relation may best describe the data, as, for example, in Figure 1.9.1.3 while in other cases the relation does not appear to be linear (e.g., Figure 1.9.1.1), or the scatter is so large that the relationship is obscured as illustrated in Figures 1.9.1.6 to 1.9.1.11 for specimens cut from large, thin-walled castings. If the DAS is averaged over selected ranges (see Figure 1.9.1.12), the scatter is reduced, but this is a subjective procedure. While there is good evidence for the dependence of F_{tu} and elongation on DAS, the determination of useful relations obviously requires considerable experience in making the measurements and in interpretation of the data.

1.9.1.1 *[Figure]* Effect of dendrite arm spacing on tensile properties of shell investment cast plates.

1.9.1.2 *[Figure]* Effect of dendrite arm spacing on tensile properties of sand-cast plates.

1.9.1.3 *[Figure]* Effect of dendrite arm spacing on tensile strength of specimens from development sand-castings.

1.9.1.4 *[Figure]* Effect of dendrite arm spacing on tensile yield strength of specimens from development sand-castings.

1.9.1.5 *[Figure]* Effect of dendrite arm spacing on tensile elongation of specimens from development sand-castings.

1.9.1.6 *[Figure]* Effect of dendrite arm spacing on tensile strength of specimens with Grade A soundness taken from sand-cast bulkheads.

1.9.1.7 *[Figure]* Effect of dendrite arm spacing on tensile yield strength of specimens with Grade A soundness taken from sand-cast bulkheads.

1.9.1.8 *[Figure]* Effect of dendrite arm spacing on tensile elongation of specimens with Grade A soundness taken from sand-cast bulkheads.

1.9.1.9 *[Figure]* Effect of dendrite arm spacing on tensile strength of specimens with Grades B and C soundness taken from sand-cast bulkheads.

1.9.1.10 *[Figure]* Effect of dendrite arm spacing on tensile yield strength of specimens with Grades B and C soundness taken from sand-cast bulkheads.

1.9.1.11 *[Figure]* Effect of dendrite arm spacing on tensile elongation of specimens with Grades B and C soundness taken from sand-cast bulkheads.

1.9.1.12 *[Figure]* Effect of dendrite arm spacing and radiographic soundness on tensile properties of development castings.

Note that the data shown represent the average of four selected DAS ranges. This subjective procedure greatly reduces the scatter in the original data.

1.9.2 Effect of impurities. The major impurity in A357.0 is iron, which has the effect of capturing a sufficient amount of magnesium in complex compounds with silicon and minor impurities to degrade the strength and to substantially reduce the elongation. The iron compounds tend to form acicular inclusions in the interdendritic structure, which probably accounts for the loss in ductility. The addition of beryllium tends to reduce the number of iron-bearing compounds and to favorably modify their morphology, off-setting to some extent the negative effects of increased iron content (Figure 1.4.3.2) (Ref. 35). However, beryllium requires special handling techniques and some foundries hesitate to use it. Recently, it has been shown (Ref. 21) that the beryllium can be eliminated, insofar as its effect on

F_{ty} is concerned. However, this reference does not give data on F_{tu} or elongation. The reduction of iron to levels below about 0.1 percent would require extreme caution in avoiding contamination from crucibles, tools, and scrap. Phosphorus has a deleterious effect, as discussed in Section 1.8.5. Other elements are generally so low in concentration that they are of no concern in premium quality castings.

1.9.3 Radiographic quality. The most frequent radiographic indications of discontinuities that are cause for rejection in aircraft castings are dross (less dense material), shrinkage sponge, and porosity (Ref. 12). Radiographs are graded as quality levels A, B, C, or D in accordance with MIL-C-6021. These quality levels are based on ASTM E 155 Reference Radiographs which provide examples of increasing severity of a given type of seven discontinuities from least detectable (No. 1) to the most severe (No. 8). For example, quality Grade B, according to MIL-C-6021, permits gas holes not exceeding those on Reference Radiograph No. 1. It should be noted that for practical purposes, industrial radiography is insensitive to discontinuities that are less than 1 percent of the part thickness. For this reason, it is not possible to qualify castings to Grade B in thicknesses over 1/2 inch. The Aluminum Association (Ref. 34) has published quality level standards for general commercial application which are less stringent than those in MIL-C-6021. For example, their highest quality level (AA) specifies Reference Radiograph No. 2 for gas holes.

For aircraft applications in critical areas, Grade B minimum is generally specified. As indicated in Tables 1.9.3.1 and 1.9.3.2 there is a substantial degradation in tensile properties of A357.0-T6 in going from Grade B to Grades C or D. High-cycle fatigue life is also substantially reduced, as shown in Figures 3.5.1.5 and 3.5.1.10. The presence of microshrinkage increases the spread of fatigue-crack propagation rates as indicated by comparison of Figures 3.5.1.9 and 3.5.1.10.

1.9.3.1 *[Table]* Effect of dross and gas porosity on tensile properties of shell investment and sand-cast plates.

1.9.3.2 *[Table]* Effect of excessive gas and shrinkage porosity on the tensile properties of sand-castings.

1.9.4 Ultrasonic inspection. Ultrasonic inspection appears useful in the detection of small amounts of dispersed gas or shrinkage porosity in castings up to 4 inches thick (Ref. 6). However, reference standards must be developed from radiographic information on material not more than 3/4-inch thick (limit of ASTM Reference Radiographs).

1.9.5 Microporosity. Reduction in tensile properties of Al-Si-Mg casting alloys has been attributed to microporosity associated with the reduction in volume during solidification (Ref. 28). This porosity may be below the threshold but can be revealed by a process using fluorescent-dye-penetrant. The casting surface is chem-milled and a plastic replica is made of the area to be examined. Using the fluorescent-dye-penetrant on the replica reveals the microporosity as small spots. It is suggested that the density of spots (number per unit area) and the size of the spots can be related to the mechanical properties of the casting (Ref. 28).

2 Physical Properties and Environmental Effects

2.1 Thermal Properties

2.1.1 Melting range: 1035 to 1135F.

2.1.2 Phase changes.

2.1.3 Thermal conductivity.

2.1.4 Thermal expansion.

68 to 212F, 11.9 in./in./F

68 to 392F, 12.5

68 to 572F, 12.9

2.1.5 Specific heat.

2.1.6 Thermal diffusivity.

2.2 Other Physical Properties

2.2.1 Density, 0.097 lb/in^3.

2.2.2 Electrical properties.

2.2.2.1 *[Figure]* Effect of aging time on the electrical conductivity and hardness of shell investment castings.

2.2.2.2 *[Figure]* Effect of aging time on the electrical conductivity and hardness of sand-castings.

2.2.2.3 Electrical resistivity, 1.71 microhm-inch.

2.2.3 Magnetic properties. Alloy is not ferromagnetic.

2.2.4 Emittance.

2.2.5 Damping capacity.

2.3 Chemical Environments

2.3.1 See Alloy 6061 (Code 3206) in this handbook.

2.4 Nuclear Environments

3 Mechanical Properties

3.1 Specified Mechanical Properties

3.1.1 *[Table]* AMS and ASTM specifications for mechanical properties and microstructure.

3.1.2 *[Table]* Military specification mechanical properties.

3.2 Mechanical Properties at Room Temperature

3.2.1 Tension – stress-strain diagrams – tension properties.

3.2.1.1 *[Figure]* Stress-strain curves for sand-cast plate.

3.2.1.2 *[Table]* Tensile, compressive, shear, and bearing properties for specimens removed from designated areas of Northrop sand-cast stepped plates from Suppliers A and B.

3.2.1.3 *[Table]* Tensile, compressive, shear, and bearing properties for specimens removed from nondesignated areas of Northrop sand-cast stepped plates from Supplier B.

3.2.1.4 *[Table]* Tensile properties and hardness of investment cast test plates.

Note that the tensile properties in this table are not always the same as those shown in related Figures 1.4.3.1, 1.5.4, 1.5.6, 1.5.8, and 1.5.10, for the nominal foundry practices and heat treatments listed here. Reasons for these discrepancies are not given in the reference. Therefore, data on each of these figures should only be used to define trends with respect to the specific independent variable in that figure.

3.2.1.5 *[Table]* Tensile properties and hardness of sand-cast test plates.

Note that the tensile properties in this table are not always the same as those shown in related Figures 1.5.5, 1.5.7, 1.5.9, and 1.5.11, for the nominal foundry practices and heat treatments listed here. Reasons for these discrepancies are not given in the reference. Therefore, data on each of these figures should only be used to define trends with respect to the specific independent variable in that figure.

3.2.1.6 *[Table]* Tensile properties of specimens removed from webs and flanges of a development casting for the F-16 vertical tail understructure.

3.2.1.7 *[Table]* Tensile properties of composite sand-cast F-16 vertical tail understructure cast at Alcoa.

3.2.1.8 *[Table]* Average tensile properties of specimens removed from two full-scale bulkheads from the Boeing Foundry.

3.2.1.9 *[Table]* Average tensile properties of specimens removed from two full-scale bulkheads from the Hitchcock Foundry.

3.2.1.10 *[Figure]* Effect of holding time at 212 or 400F on tensile properties at room temperature

3.2.1.11 *[Figure]* Configuration of double-ligament tensile (DLT) specimen in test rig used to measure anisotropy in mechanical properties of cylindrical sand-castings.

3.2.1.12 *[Table]* Effect on tensile properties of specimen orientation with respect to axis of sand-cast cylinders.

Only ultimate strength and elongation in the tangential orientation are significantly affected.

3.2.1.13 *[Table]* Smooth tensile, notch tensile and fatigue toughness properties of specimens from sand composite cast plates from three suppliers and from F5 wing pylons.

3.2.1.14 *[Table]* Smooth tensile and fracture toughness properties of specimens from sand composite cast plates with intentional defects.

3.2.2 Compression – stress-strain diagrams – compression properties (See Tables 3.2.1.2 and 3.2.1.3).

3.2.2.1 *[Figure]* Compressive stress-strain curve for sand-cast plate.

3.2.3 Impact.

3.2.4 Bending.

3.2.5 Torsion and shear (see Tables 3.2.1.2 and 3.2.1.3).

3.2.6 Bearing (see Tables 3.2.1.2 and 3.2.1.3).

3.2.7 Stress concentration.

3.2.7.1 Notch properties.

3.2.7.2 Fracture toughness (see also Tables 3.2.1.13, 3.2.1.14 and 4.3.1.2).

3.2.7.2.1 General. Attempts to measure the plane-strain fracture toughness, K_{Ic}, in accordance with ASTM E 399 have met with little success. Frequently specimens removed from a casting are of insufficient thickness to measure a valid K_{Ic}. This, per se, is not a basic problem if the specimen represents essentially the full thickness of the section being examined. In fact, this is a good finding and indicates that fracture of the part will probably not be controlled by plane-strain fracture. However, in most cases where the thickness is sufficient, valid values of K_{Ic} cannot be obtained because of excess fatigue-crack front curvature. (e.g., see Tables 3.2.7.2.2 and 3.2.7.2.3). In these examples, the primary cause of invalid values was crack front curvature. The excessive crack front curvature in castings is due to a combination of residual stresses associated with quenching from the solution temperature and to the nonuniform microstructure, which is generally finer at the surface due to a more rapid solidification rate. Various remedies for this curvature problem have been suggested including lateral compression and

side grooving. Side grooving will probably help, but removes part of the material in the casting. However, if the material removed does have a superior microstructure to that remaining, it may be speculated that the side-grooved specimen will yield underestimates of the true fracture resistance of the actual part.

A few valid values of K_{Ic} have been reported (see Table 3.2.7.2.2) which vary from about 16 to 19 ksi $\sqrt{in}$. It is not clear whether or not the casting from which these specimens were taken represent D357.0 as presently defined in the AMS specification. Values as low as 13 ksi $\sqrt{in}$. have been suggested for design (Ref. 13). In light of more recent K_Q values (e.g., Table 3.2.7.2.4) such a design value seems rather low. K_Q values obtained from intentionally defective step plates with severe sponge shrinkage (Table 3.2.7.2.6) show no significant difference from plates having radiographic Grade B or better. Tests at -65F on the same type of specimens as represented in Table 3.2.7.2.2 did not reveal any difference between K_Q at -65 or at room temperature. This behavior would be expected for most aluminum alloys.

3.2.7.2.2 *[Table]* Results of tests on ASTM E 399 compact specimens removed from separately sand-cast blocks.

3.2.7.2.3 *[Table]* Results of tests on ASTM E 399 compact specimens removed from separately sand-cast bulkhead lugs.

3.2.7.2.4 *[Table]* Results of tests on ASTM E 399 compact specimens removed from separately sand-cast blocks and from designated areas of stepped plates.

3.2.7.2.5 *[Table]* Results of tests on ASTM E 399 compact specimens removed from full-scale F-16 vertical tail understructure.

3.2.7.2.6 *[Table]* Fracture toughness of specimens removed from intentionally produced defective step plates.

3.2.8 Combined properties

3.3 Mechanical Properties at Various Temperatures

3.3.1 Tension – stress-strain diagrams – tension properties.

3.3.1.1 *[Figure]* Effect of test temperature and holding time on tensile properties.

3.3.1.2 *[Figure]* Effect of elevated test temperature on tensile properties of sand-castings.

3.3.2 Compression – stress-strain diagrams – compression properties.

3.3.3 Impact.

3.3.4 Bending.

3.3.5 Torsion and shear.

3.3.6 Bearing.

3.3.7 Stress concentration.

3.3.7.1 Fracture toughness.

3.3.8 Combined properties.

3.4 Creep and Creep Rupture Properties

3.4.1 *[Figure]* Creep and creep rupture at 350F.

3.5 Fatigue Properties

3.5.1 Conventional high-cycle fatigue.

3.5.1.1 *[Figure]* S-N curves for axial fatigue of separately sand-cast test specimens.

3.5.1.2 *[Figure]* S-N curves for smooth and notched specimens.

3.5.1.3 *[Figure]* S-N curves at elevated temperature for specimens removed from sand-cast stepped plates.

3.5.1.4 *[Figure]* S-N curves for notched specimens from sand-castings.

3.5.1.5 *[Figure]* Effect of sponge shrinkage (Grade C) and round gas porosity (Grade D) on notched fatigue properties of sand-castings.

3.5.1.6 *[Table]* Smooth and notched fatigue properties of separately sand-cast specimens and specimens removed from cast bulkhead.

3.5.1.7 *[Figure]* S-N curves for smooth specimens from composite sand-cast plates from three suppliers and specimens from F5 wing pylon.

Maximum stresses for materials from Foundries B and C are significantly lower than for Foundry A material for the same high-cycle fatigue lives. Referring to the tensile properties in Table 3.2.1.13, only the lower NTS/F_{ty} ratios of Foundries B and C material correlate with these fatigue results. Good correlation was found between the fatigue lives of specimens from full-scale F5 wind pylon castings and those of plate castings, both from Foundry A.

3.5.1.8 *[Figure]* S-N curves for notched specimens from composite sand-cast plates from three suppliers.

Little difference between foundries is seen in fatigue lives with stress concentrations.

3.5.1.9 *[Figure]* Effect of gas porosity on S-N curves for smooth specimens from composite sand-cast plates.

Metal was not de-gassed in order to introduce the porosity. Grades B and C porosities averaged 1.1 and 1.7 percent, respectively, with bubble aspect ratios of approximately 2. Grade D porosity was not reported. For a fatigue life of 10^7 cycles, Grade B porosity reduced maximum stress about 30 percent, compared to the baseline material without porosity, while reductions for Grades C and D materials were about 60 percent.

3.5.1.10 *[Figure]* Effect of shrinkage porosity on S-N curves for smooth specimens from composite sand-cast plates.

Shrinkage porosity levels were approximately the same as gas porosity levels, but were non-spherical. Effects on Grade B material fatigue resistance were somewhat more detrimental than gas porosity (see Figure 3.5.1.9). Reductions in the fatigue lives of Grade C material were approximately the same from shrinkage porosity as from gas porosity.

3.5.1.11 *[Figure]* Effect of dross on S-N curves for smooth specimens from composite sand-cast plates.

Grades B and C dross porosity at 1.6 to 0.6 percent levels, respectively, reduced high-cycle fatigue lives as much as Grade C gas and shrinkage porosity at slightly higher levels.

3.5.2 Low-cycle-fatigue.

3.5.2.1 *[Figure]* Strain-fatigue life curve for smooth specimens from composite sand-cast plates from three suppliers.

Unlike fatigue resulting from stress-cycling (see Figure 3.5.1.7), strain-cycle fatigue data from the three foundries are indistinguishable. While not reported in the reference, this probably is the result of a cyclic strain softening behavior, in which maximum stress decreases with continued strain cycling, but maximum strain increases with continued stress cycling. Correlation of the fatigue lives for two R ratios (-1 and 0.1) on the basis of maximum strain is reasonable.

3.5.3 Fatigue-crack propagation.

3.5.3.1 *[Figure]* Fatigue-crack growth rates for specimens removed from designated areas in sand-cast stepped plates.

3.5.3.2 *[Figure]* Fatigue-crack growth rates at 250 and 400F for specimens removed from designated areas in sand-cast stepped plates.

3.5.3.3 *[Figure]* Scatter bands of fatigue-crack growth rates for specimens removed from a cast bulkhead.

3.5.3.4 *[Figure]* Scatter band of fatigue-crack growth rates for specimens removed from a cast bulkhead in shear web areas exhibiting microshrinkage.

3.5.3.5 *[Table]* Measures of the variability in cycles required to grow a crack from an initial to a final value (derived from tests on seven s pecimens).

3.5.3.6 *[Figure]* Fatigue-crack growth rates in lab air and in high humidity for specimens removed from full-scale F-16 vertical tail substructure.

3.5.3.7 *[Figure]* Fatigue-crack growth rates at several R-ratios for specimens removed from full-scale F-16 vertical tail substructure.

3.5.3.8 *[Figure]* Fatigue-crack growth rates for specimens removed from full-scale F-16 vertical tail substructure.

3.5.3.9 *[Figure]* Scatter bands of fatigue-crack growth rates for specimens from composite sand-cast plates from three suppliers, for water- and glycol-quenched conditions.

Crack growth is slower for glycol-quenched material, but with greater scatter. Differences between materials from different suppliers were not significant.

3.5.3.10 *[Figure]* Scatter band of fatigue-crack growth rates for specimens cut from a F5 aircraft wing pylon, compared with plate specimen growth rates.

Growth rates for full-scale pylon casting specimens were in excellent agreement with those from plate casting specimens.

3.5.3.11 *[Figure]* Effects of gas porosity on fatigue-crack growth rates of specimens from cast plates.

3.5.3.12 *[Figure]* Effects of gas porosity or dross on fatigue-crack growth rates of specimens from cast plates.

3.6 Elastic Properties

3.6.1 Poisson's ratio.

3.6.2 Modulus of elasticity.

3.6.2.1 *[Figure]* Effect of temperature on tensile modulus of elasticity.

3.6.3 Modulus of rigidity.

3.6.4 Tangent modulus.

3.6.5 Secant modulus.

4 Fabrication

4.1 Forming

4.2 Machining and Grinding

4.3 Joining

4.3.1 Welding.

4.3.1.1 General. The alloy may be welded in any temper. However, where joining of sections is done by welding it is advisable to do this in the as-cast (F) or annealed condition (T2) where the ductility is high and then to heat treat the assembly to the T6 condition (Ref. 37). This sequence results in stress relief. Repair welding of castings containing localized areas of shrinkage, porosity, or dross can be accomplished using wire conforming to AMS 4246B. Repair welds may be made in fully heated casting if the reduction in mechanical properties is not detrimental to the performance, as in an area where the stresses are low (Ref. 38). If cracking occurs during repair welding the entire casting should be annealed before further repair is attempted.

Simulated weld repairs were made in the Northrop programs. In one case (Ref. 12) the welds were made in grooves cut into designated areas of the step plates with no intentional defects and specimens were abstracted from these plates such that the gauge sections contained substantial amounts of the weld material (see Figure 4.3.1.2). In another case (Ref. 41) the weld grooves were machined into 16 x 16 x 1.25-in. cast plates containing intentional defects. In both cases the plates were heat treated to the T6 condition after welding. Tensile tests on weld-containing specimens from plates with no intentional defects (Table 4.3.1.3) show properties essentially equal to the unwelded metal. Fracture toughness data based on K_Q also indicate no difference between welded and unwelded specimens. On the other hand, differences are observed in the notch fatigue strength (Figure 4.3.1.5), with the welded specimens having shorter lives in the range above about 10^5 cycles. Fatigue-crack growth rates (Figure 4.3.1.6) for welded specimens scatter considerably but appear to be higher than those for unwelded specimens.

4.3.1.2 *[Figure]* V-grooved (60-degree V, 0.25-inch deep with 3/32-inch radius) weld specimens from Northrop stepped plates.

Welding procedure reported as "normal" to fill the groove.

4.3.1.3 *[Table]* Effect of weld repairs on tensile properties and fracture toughness of specimens from stepped plate sand-castings.

4.3.1.4 *[Figure]* Effect of weld repairs on fatigue strength of smooth specimens from composite sand-cast stepped plates, compared with the effects of gas porosity alone.

4.3.1.5 *[Figure]* Effect of weld repairs on fatigue strength of notched specimens from stepped plate sand-castings.

4.3.1.6 *[Figure]* Effect of weld repairs on fatigue-crack growth rates of specimens from sand-cast plates with Grade B gas porosity.

4.3.2 Bonding.

4.3.2.1 The effect of the as-cast surface finish of A357.0-T6 adherends on the relative strengths of bond joints was investigated using single-shear lap tests and comparing the cast specimen results with comparable results for machined 2024-T3 adherends (Ref. 36). Surface preparation and bonding procedures were the same for both the A357.0-T6 and 2024-T3 alloys. Two adhesive systems, dry and wet environments, and several test temperatures were included in the test program. Ratios of the lap-bond strength of the as-cast adherends to that of the machined adherends varied from 0.65 to 1.24.

4.3.2.2 *[Table]* Single-shear lap bond strength of as-cast A357.0-T6 adherends with two adhesive systems.

4.3.2.3 *[Table]* Surface preparation and bonding procedures for fabrication of lap joint test specimens.

Table 1.4.2 AMS and ASTM composition for A357.0 and D357.0

Alloy	357.0, A357.0 and D357.0											
Specification	AMS 4219C, MIL-A-11180D, ASTM B 686		AMS 4249		AMS 4241A		AMS 4246B		ASTM B 108		ASTM B 108	
Reference	1, 45, 46		2		43		44		45		45	
Designation[c]	A357.0-T61		D357.0-T6		D357.0-T6		357		A357.0		357.0	
UNS	A13570		A43570		A43570		A03570		A13570		A03570	
Grade/Type	Aircraft Quality		Damage Tolerant[a] Aircraft Quality		DAS Controlled[b] Aircraft Quality		Weld Wire		Permanent Mold Castings		Permanent Mold Castings	
Composition	Minimum	Maximum	Minimum	Maximum	Minimum	Maximum	Minimum	Maximum	Minimum	Maximum	Minimum	Maximum
Si	6.5	7.5	6.5	7.5	6.5	7.5	6.5	7.5	6.5	7.5	6.5	7.5
Mg	0.40	0.7	0.55	0.6	0.55	0.6+	0.45	0.6	0.4	0.7	0.45	0.6
Ti	0.04	0.20	0.10	0.20	0.10	0.20	—	0.20	0.04	0.2	—	0.2
Be	0.04	0.07	0.04	0.07	0.04	0.07	—	0.15	—	—	—	—
Fe	—	0.20	—	0.12	—	0.12	—	0.05	—	0.2	—	0.15
Cu	—	0.20	—	—	—	—	—	0.05	—	0.2	—	0.05
Mn	—	0.10	—	0.10	—	0.10	—	0.03	—	0.1	—	0.03
Zn	—	0.10	—	—	—	—	—	0.05	—	0.1	—	0.05
Other, each	—	0.05	—	0.05	—	0.05	—	0.05	—	0.05	—	0.05
Other, total	—	0.15	—	0.15	—	0.15	—	0.15	—	0.15	—	0.15

[a] Requires fatigue and fracture toughness and DAS ≤ 0.002 inch.

[b] DAS measurements are used to arrive at the specified mechanical properties.

[c] Designations established by the Aluminum Association and adopted by AMS.

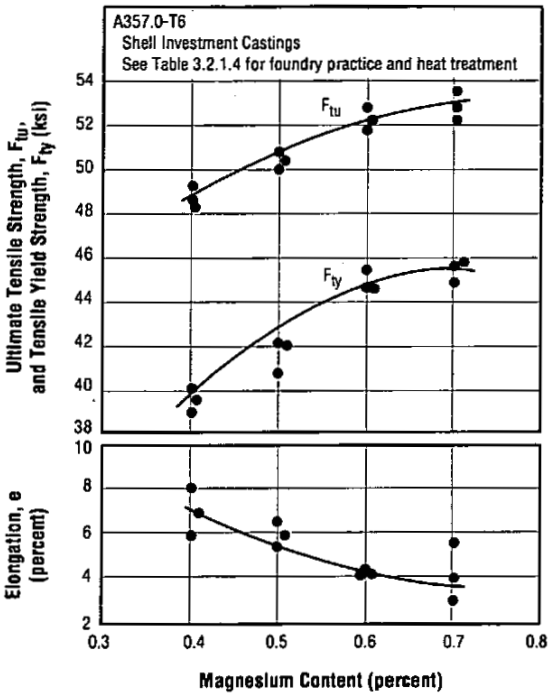

Figure 1.4.3.1 Effect of magnesium content on the tensile properties of shell investment castings (Ref. 12)

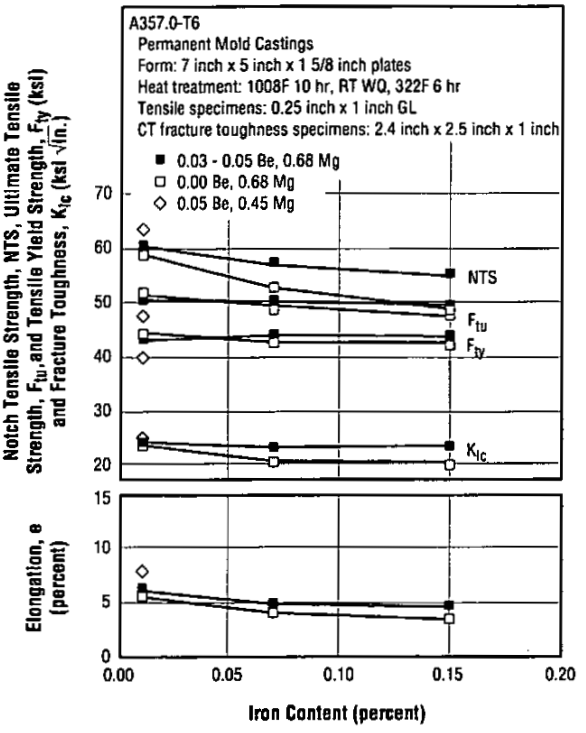

Figure 1.4.3.2 Effects of iron, beryllium, and magnesium contents on tensile and fracture properties of plates cast in permanent molds (Ref. 35)

Table 1.4.3.3 Average tensile, notch yield strength ratio, and percent porosity for specimens cut from cast blocks produced with two chill rates and aged at two temperatures (Ref. 41)

Alloy	D357.0-T6			
Composition	AMS 4219C (except Mg 0.55-0.6) Eight variations within specification limits			
Form	6 inch x 12 inch x 0.75 inch Sand Castings			
Si Modifier	Sr			
Mold and Pour Conditions	Slow Cool: Fe chill + 1440F pour temperature Average DAS = 2.0 mils DAS range = 1.4 - 2.7 mils Fast Cool: Cu chill + 1380F pour temperature Average DAS = 2.3 mils DAS range = 1.5 - 2.9 mils			
Solution Treat	1010F 16 hr, RT, WQ			
Age	315F 12 hr or 335F 6 hr			
Radiographic Quality	Grade B or better			
Test Replications	1 per composition/age/chill combination			
Average Properties	Fe chill		Cu chill	
	315F 12 hr	335F 6 hr	315F 12 hr	335F 6 hr
F_{tu} (ksi)	50	51	52	53
F_{ty} (ksi)	42	44	42	45
e (percent)	4.3	3.8	6.4	6.0
NTS/F_{ty} [a]	1.21	1.15	1.28	1.20
Porosity (percent)	0.047	0.024	0.007	0.015

[a] Notch tensile, ASTM E 602, 0.5-inch diameter specimen.

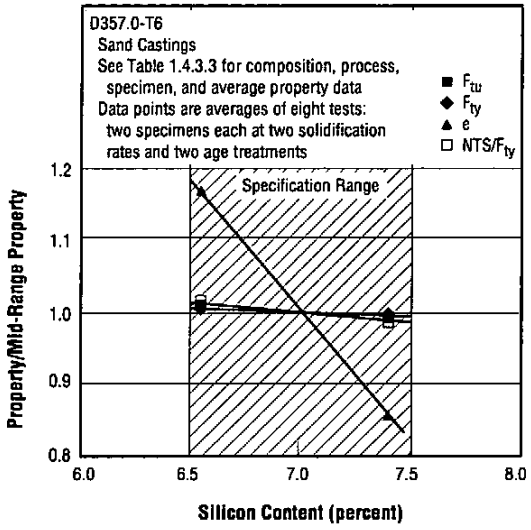

Figure 1.4.3.4 Relative effects of silicon content on tensile properties of D357.0-T6 sand castings (Ref. 41)

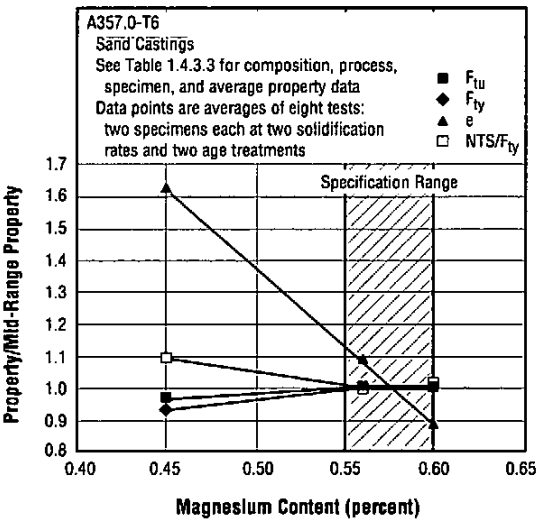

Figure 1.4.3.5 Relative effects of magnesium content on tensile properties of D357.0-T6 sand castings (Ref. 41)

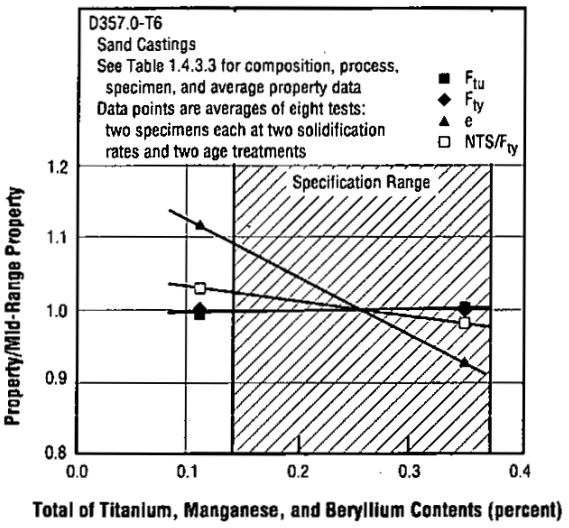

Figure 1.4.3.6 Relative effects of the combined titanium, manganese, and beryllium contents on tensile properties of D357.0-T6 sand castings (Ref. 41)

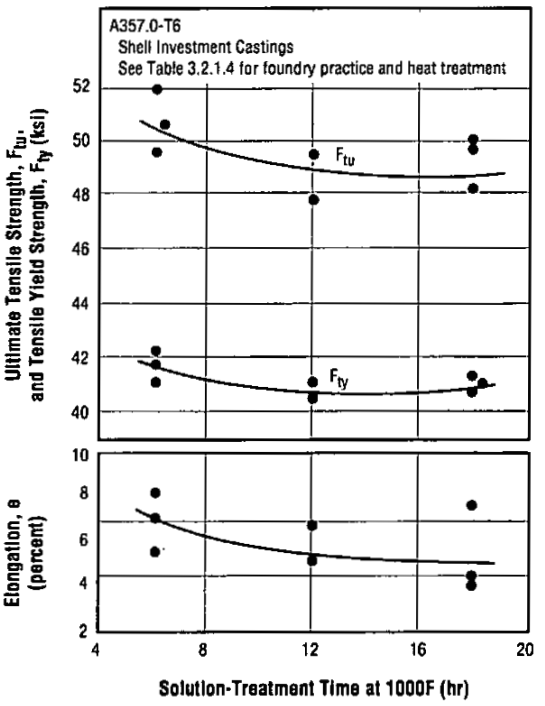

Figure 1.5.4 Effect of solution-treatment time on tensile properties of shell investment castings (Ref. 12)

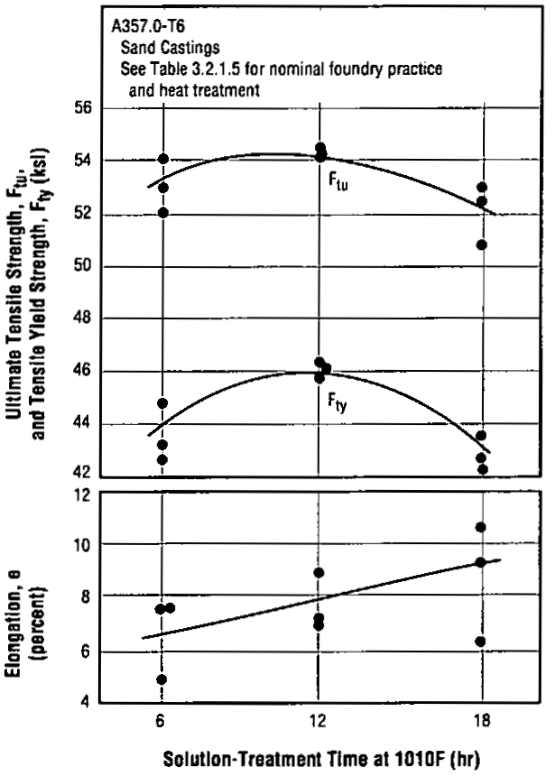

Figure 1.5.5 Effect of solution-treatment time on tensile properties of sand castings (Ref. 12)

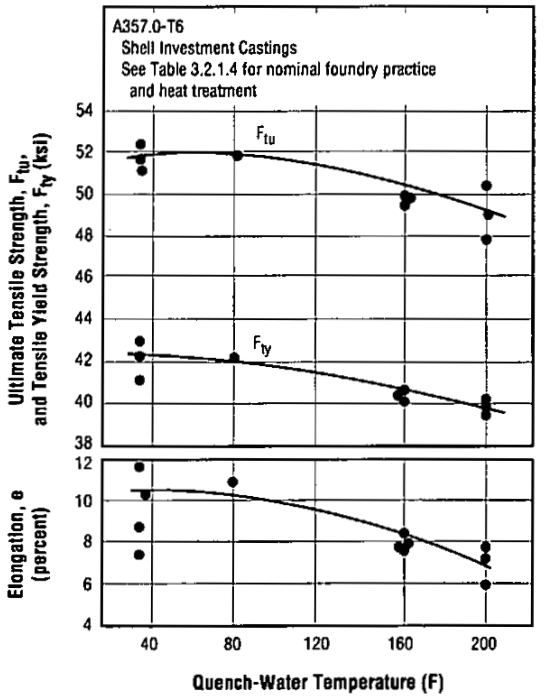

Figure 1.5.6 Effect of quench-water temperature on tensile properties of shell investment castings (Ref. 12)

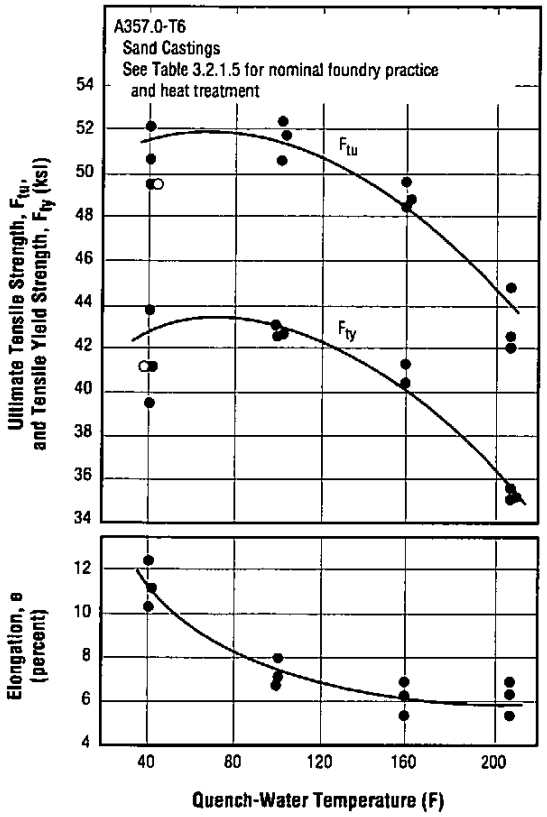

Figure 1.5.7 Effect of quench-water temperature on tensile properties of sand castings (Ref. 12)

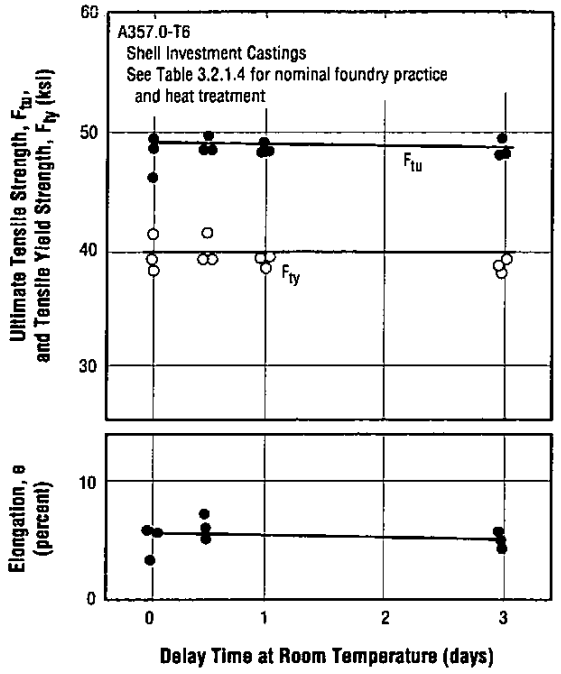

Figure 1.5.8 Effect of delay time between solution treatment and quench for shell investment castings (Ref. 12)

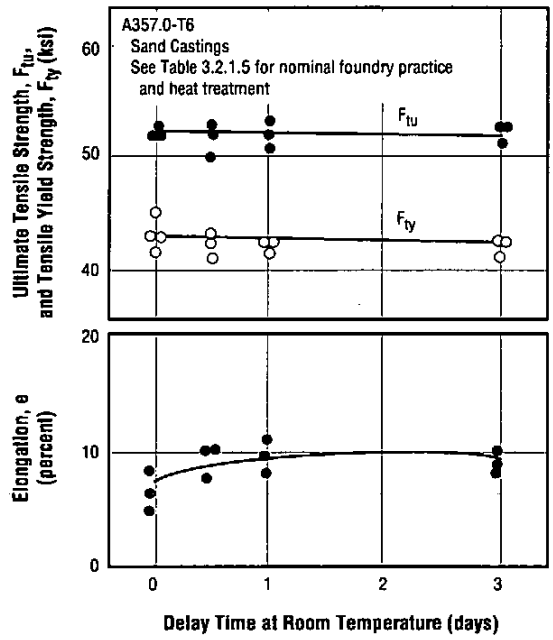

Figure 1.5.9 Effect of delay time between solution treatment and quench for sand castings (Ref. 12)

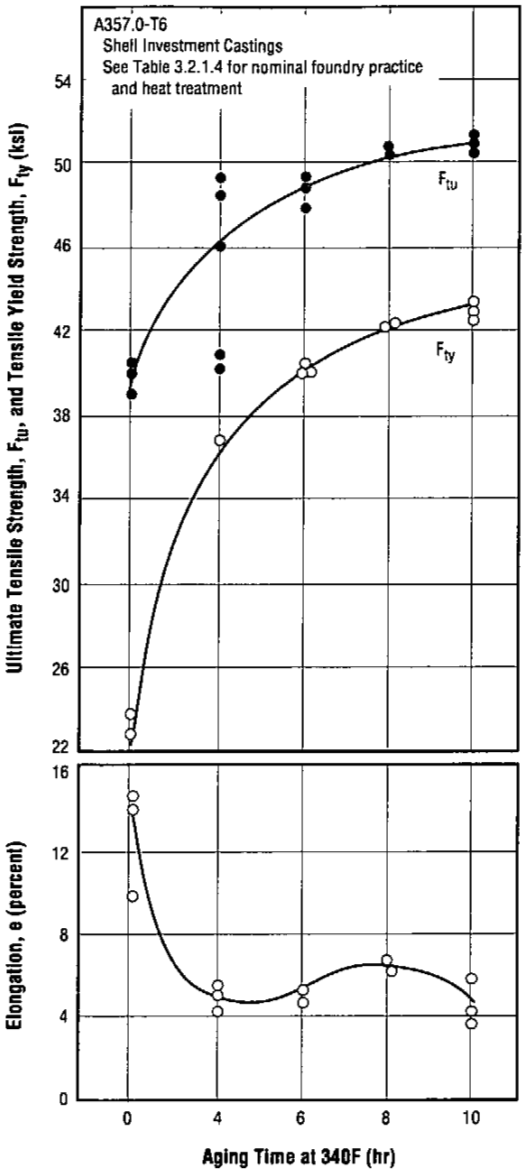

Figure 1.5.10 Effect of aging time on tensile properties of investment castings (Ref. 12)

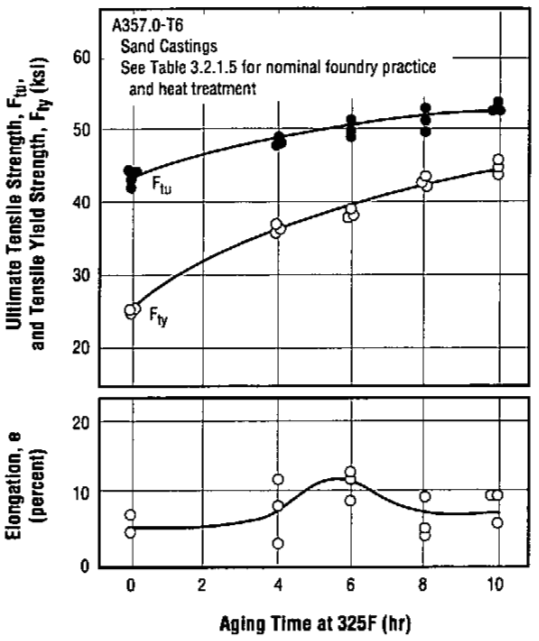

Figure 1.5.11 Effect of aging time on tensile properties of sand castings (Ref. 12)

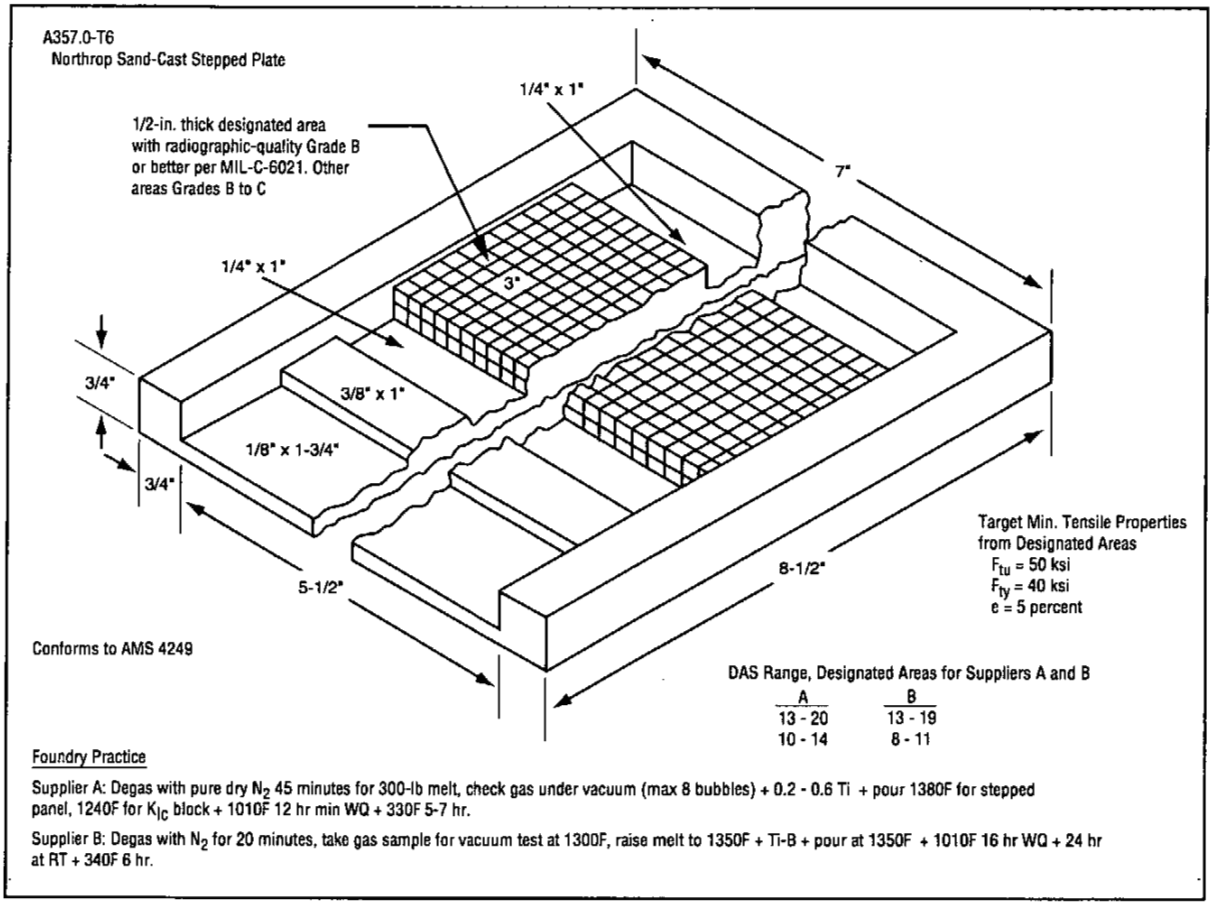

Figure 1.8.1.1 Sand-mold stepped-plates configuration used in the Northrop program to determine design property data for sand-cast A357.0-T6 from two suppliers: A (Magnesium Alloy Products) and B (Teledyne Cast Products). Two integal tensile coupons attached at optional locations. (Ref. 12)

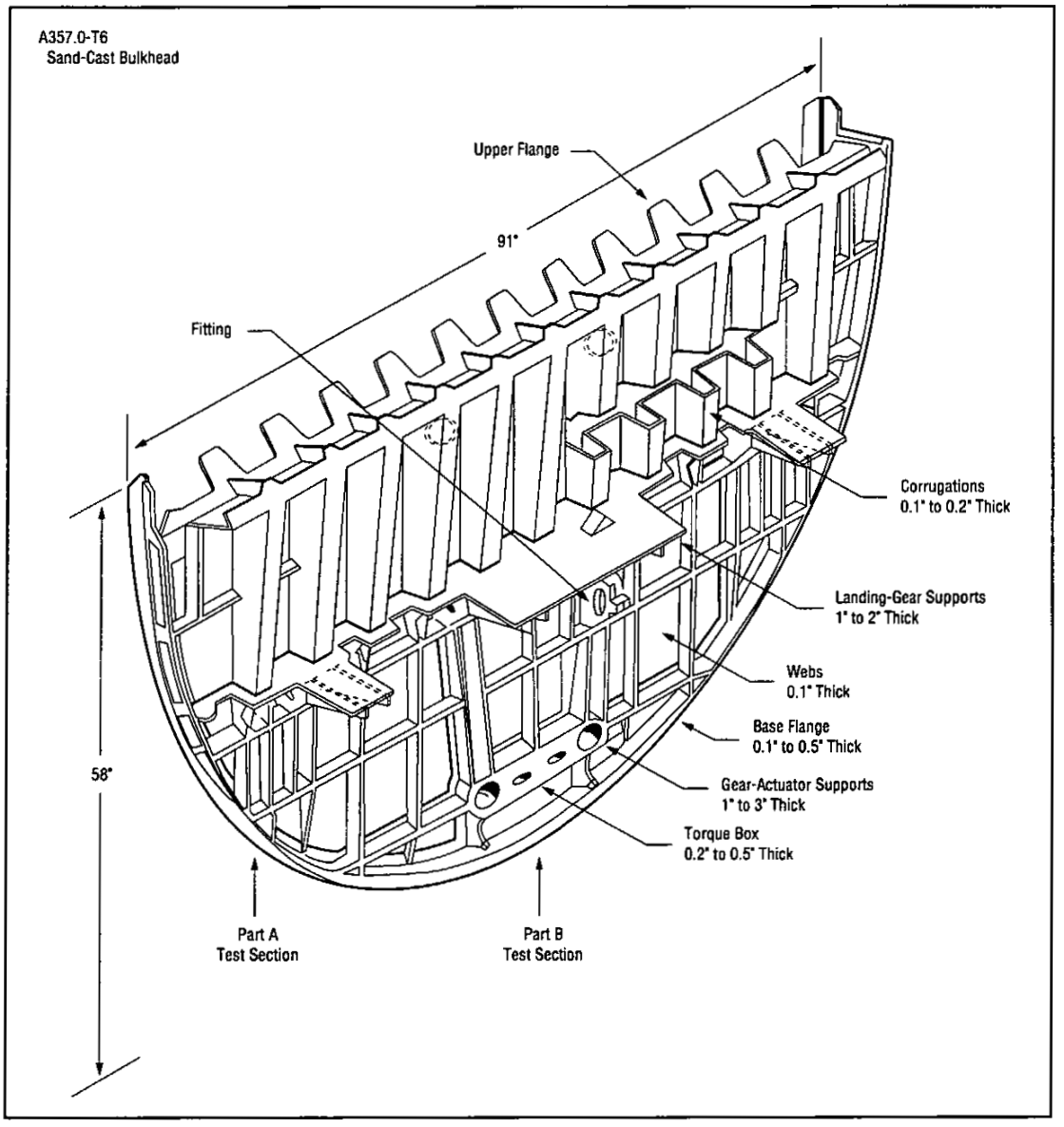

Figure 1.8.1.2 Large, thin-walled, composite sand-cast nose-gear support bulkhead for the YC-14 airplane. Ten identical castings were each produced by the Boeing and the Hitchcock Foundries using Boeing-developed manufacturing plans and tooling (Ref. 10)

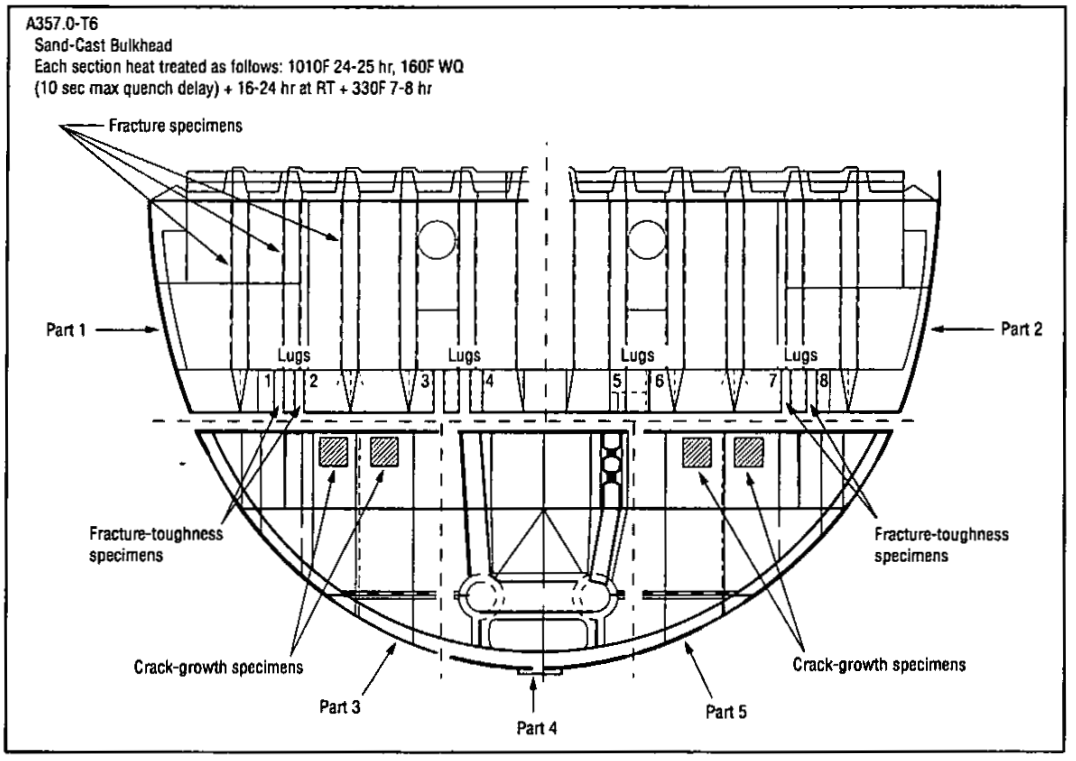

Figure 1.8.1.3 Nose landing-gear support bulkhead casting showing locations of specimens removed from five sections of the casting (Each section heat treated separately) (Ref. 7)

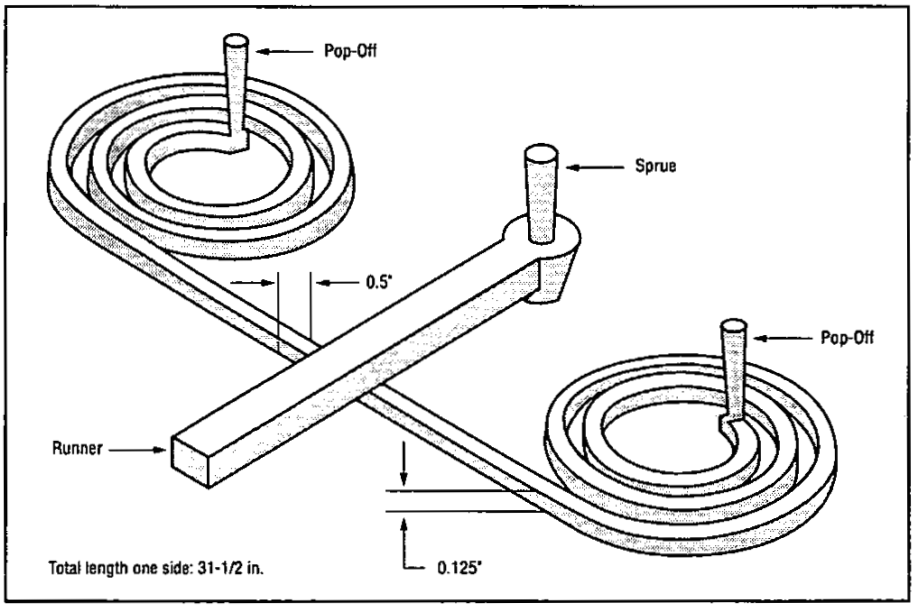

Figure 1.8.2.1 Double spiral fluidity test casting (Ref. 10)

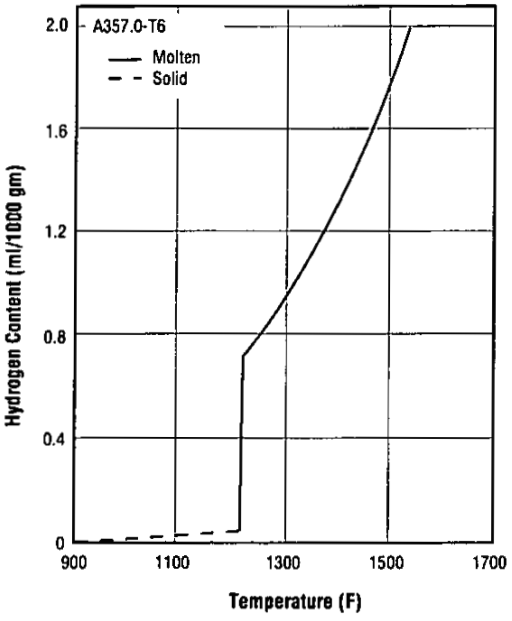

Figure 1.8.4.1 Solubility of hydrogen in solid and molten aluminum as a function of temperature (Ref. 10)

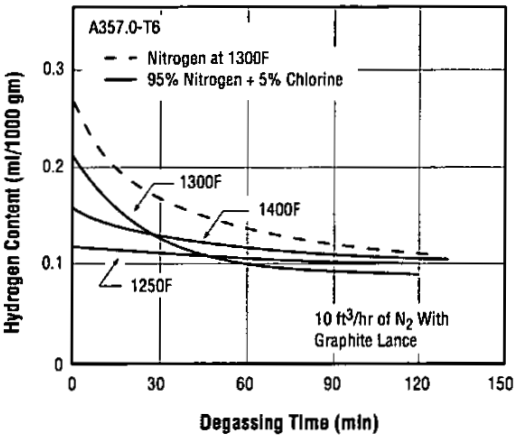

Figure 1.8.4.2 Effect of degassing time and temperature on hydrogen content (Ref. 5)

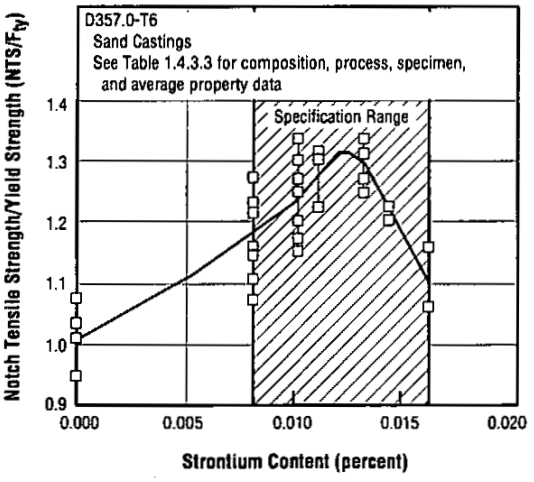

Figure 1.8.5.1 Effect of strontium content on the ratio of notched tensile strength to tensile yield strength of D357.0-T6 sand castings (Ref. 41)

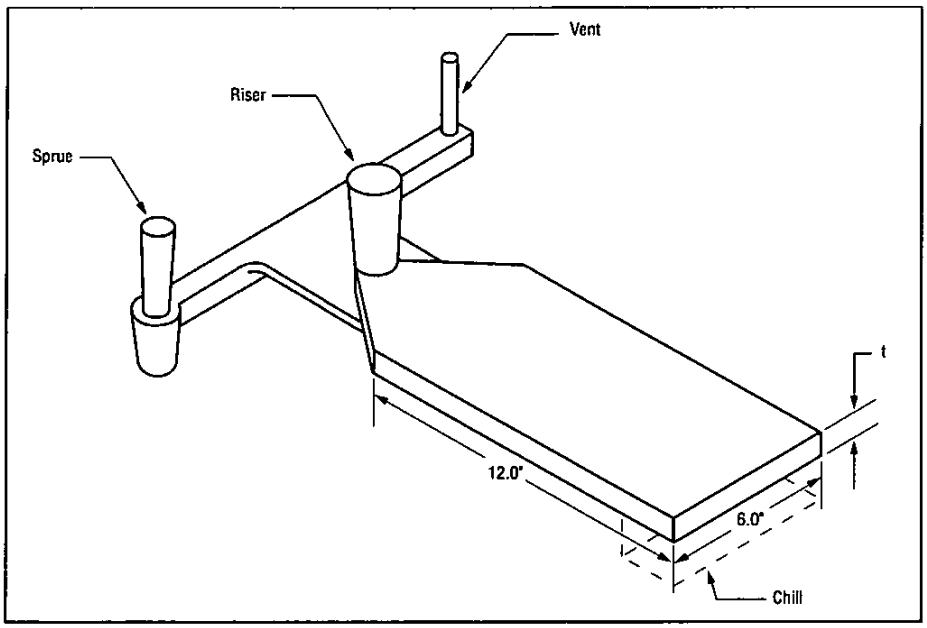

Figure 1.8.6.1 Test plate configuration incorporating a chill (Ref. 5)

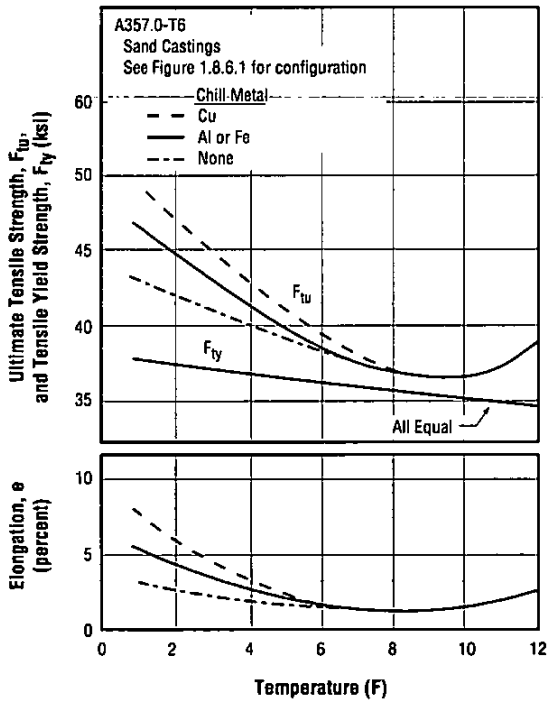

Figure 1.8.11.1 Effect of various chill metals and distance from the chill for sand castings (Ref. 5, Figures 55, 56)

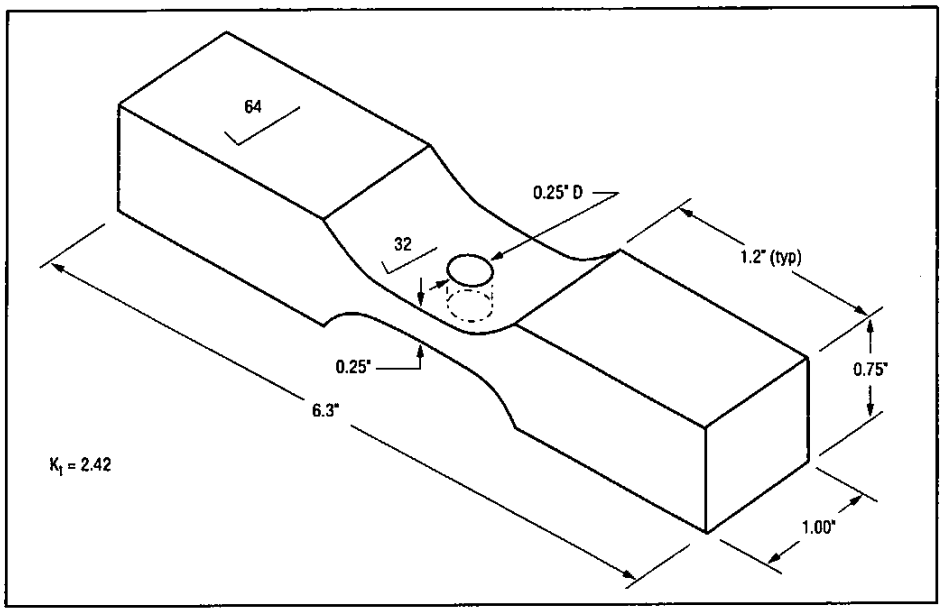

Figure 1.8.11.2 Configuration of fatigue test specimen used to measure the effects of chill rates and aging processes on high-cycle fatigue life (Ref. 41)

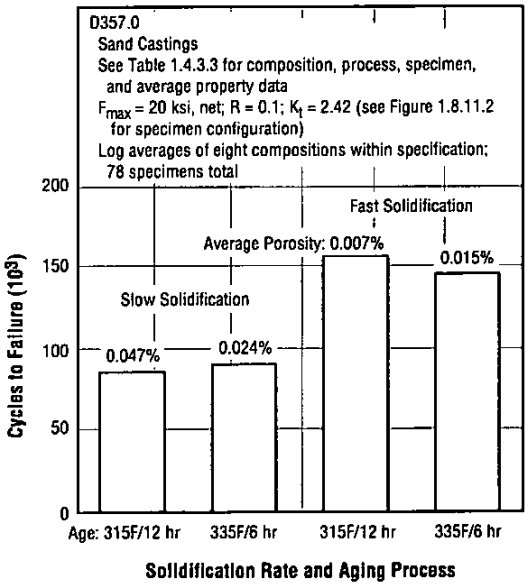

Figure 1.8.11.3 Effect of chill rates and aging proceses on tension-tension fatigue life of notched specimens of D357.0 alloy at 20 ksi maximum stress (Ref. 41)

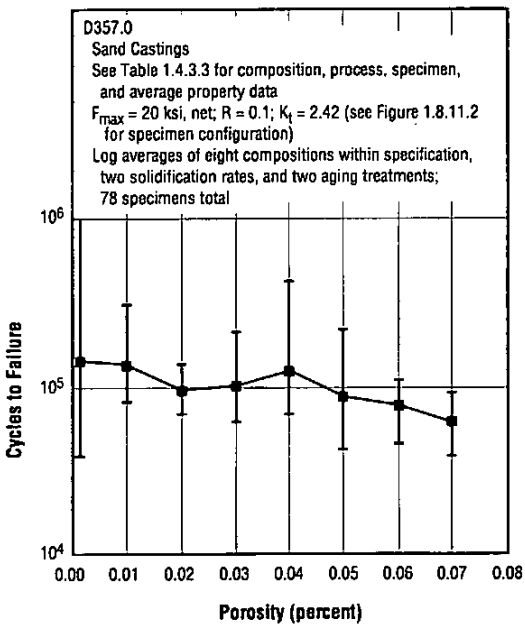

Figure 1.8.11.4 Effect of porosity from different chill rates and aging processes on tension-tension fatigue life of notched specimens of D357.0 alloy at 20 ksi maximum stress (Ref. 41)

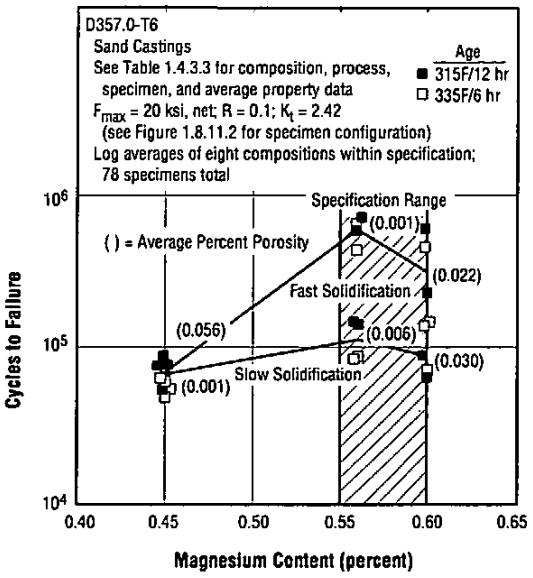

Figure 1.8.11.5 Effect of magnesium content on tension-tension fatigue life of notched specimens of D357.0 alloy at 20 ksi maximum stress, with different chill rates and aging processes (Ref. 41)

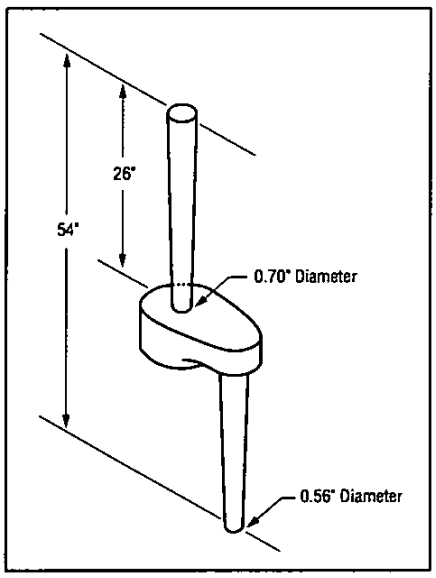

Figure 1.8.12.1 Cascading sprue designed to combine good hydrostatic head with minimum turbulence (Ref. 5)

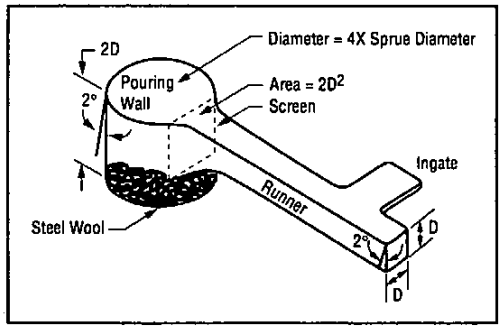

Figure 1.8.12.2 Basic features of pouring well, runner, and ingate (Ref. 5)

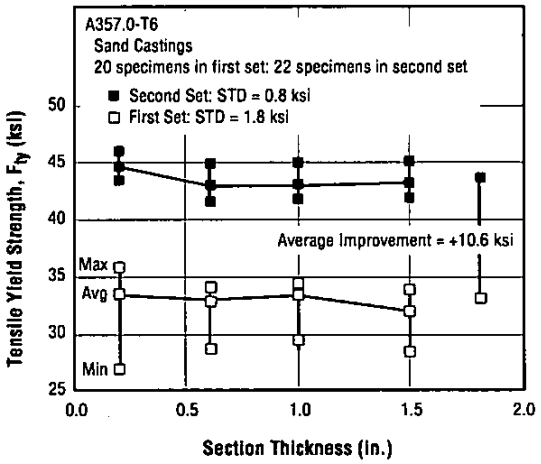

Figure 1.8.13.1 Improvement in tensile yield strength from the first to the second set of sand castings (Ref. 40)

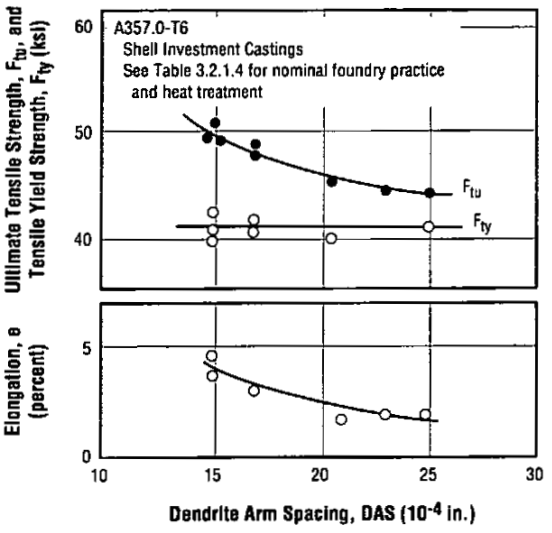

Figure 1.9.1.1 Effect of dendrite arm spacing on tensile properties of shell investment cast plates (Ref. 12)

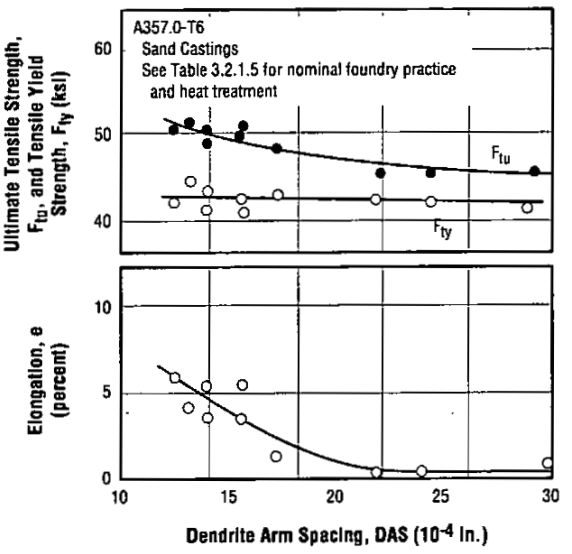

Figure 1.9.1.2 Effect of dendrite arm spacing on tensile properties of sand-cast plates (Ref. 12)

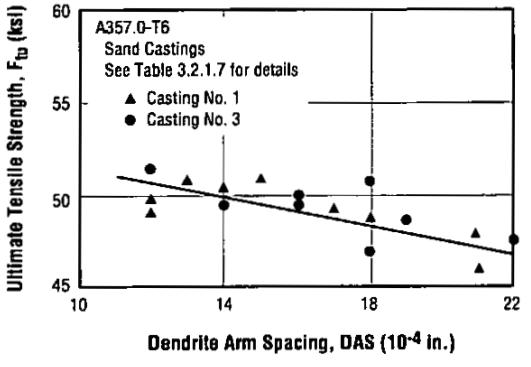

Figure 1.9.1.3 Effect of dendrite arm spacing on tensile strength of specimens from development sand castings (Ref. 13)

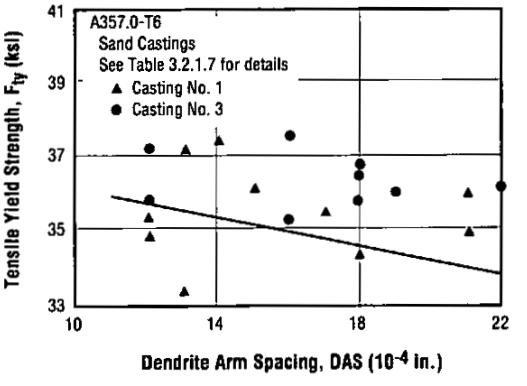

Figure 1.9.1.4 Effect of dendrite arm spacing on tensile yield strength of specimens from development sand castings (Ref. 13)

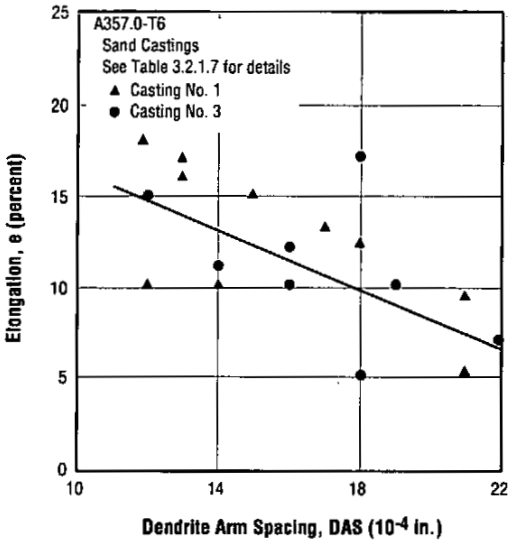

Figure 1.9.1.5 Effect of dendrite arm spacing on tensile elongation of specimens from development sand castings (Ref. 13)

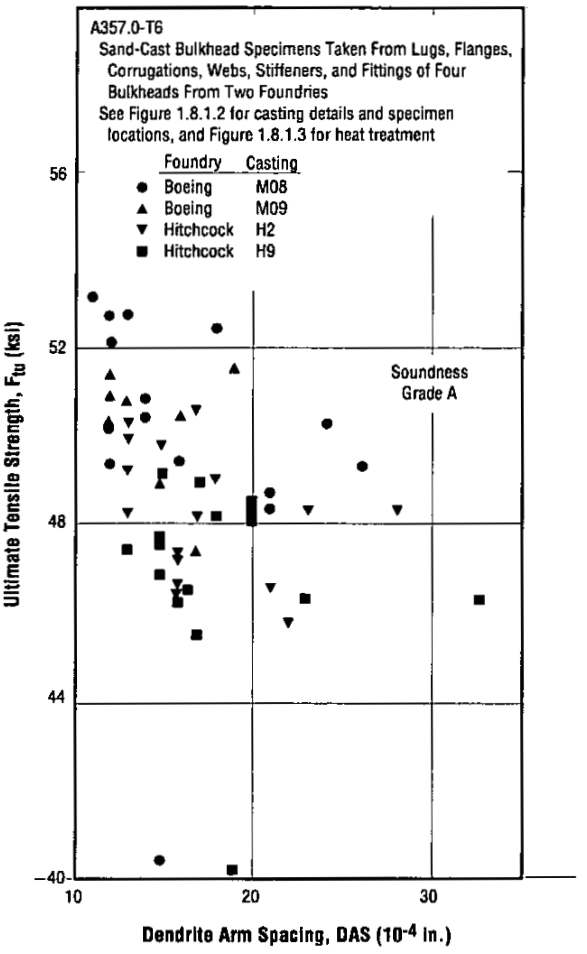

Figure 1.9.1.6 Effect of dendrite arm spacing on tensile strength of specimens with Grade A soundness taken from sand-cast bulkheads (Ref. 10)

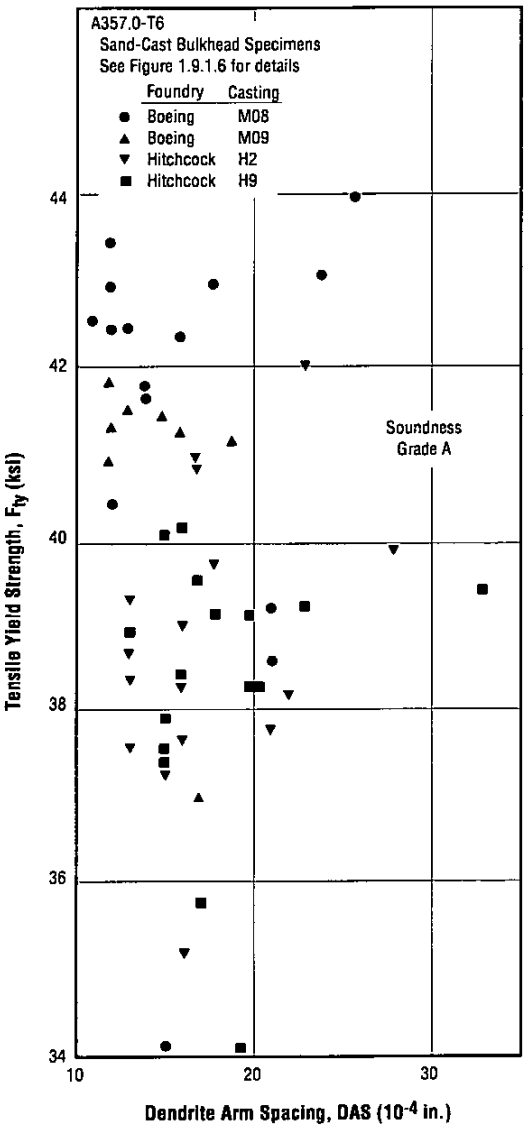

Figure 1.9.1.7 Effect of dendrite arm spacing on tensile yield strength of specimens with Grade A soundness taken from sand-cast bulkheads (Ref. 10)

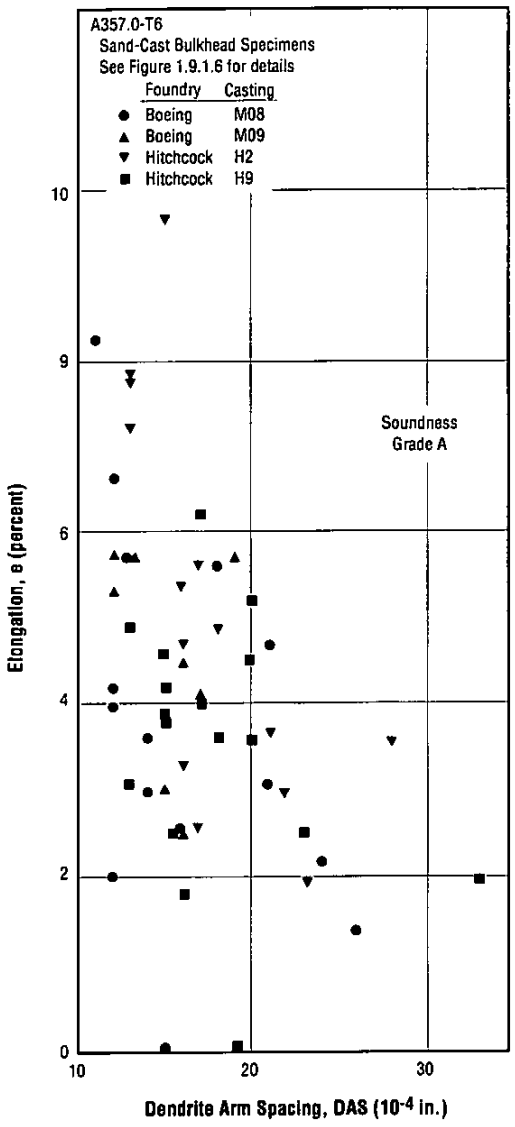

Figure 1.9.1.8 Effect of dendrite arm spacing on tensile elongation of specimens with Grade A soundness taken from sand-cast bulkheads (Ref. 10)

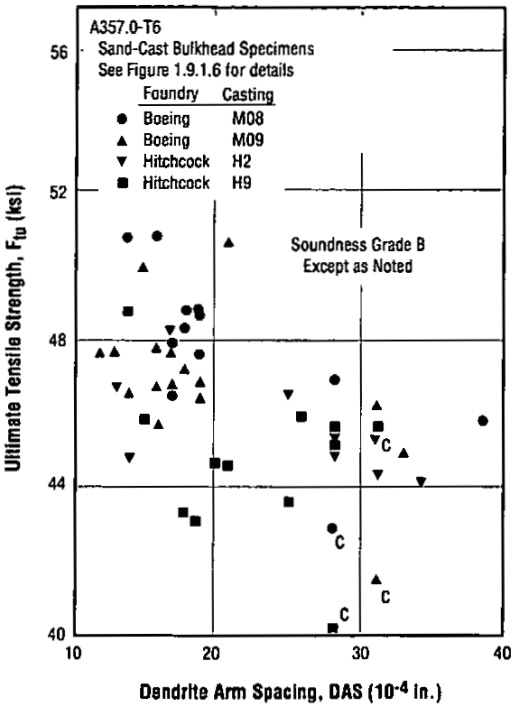

Figure 1.9.1.9 Effect of dendrite arm spacing on tensile strength of specimens with Grades B and C soundness taken from sand-cast bulkheads (Ref. 10)

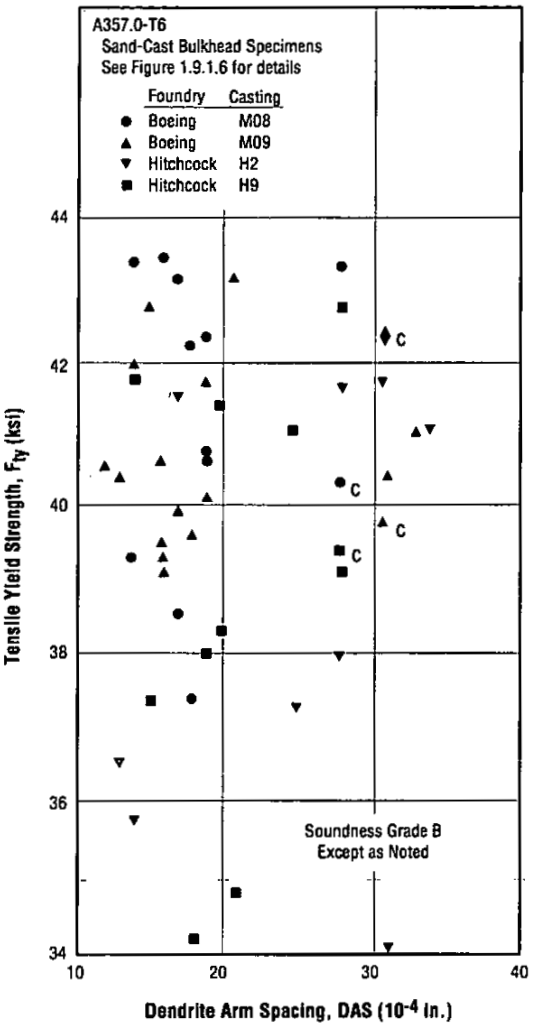

Figure 1.9.1.10 Effect of dendrite arm spacing on tensile yield strength of specimens with Grades B and C soundness taken from sand-cast bulkheads (Ref. 10)

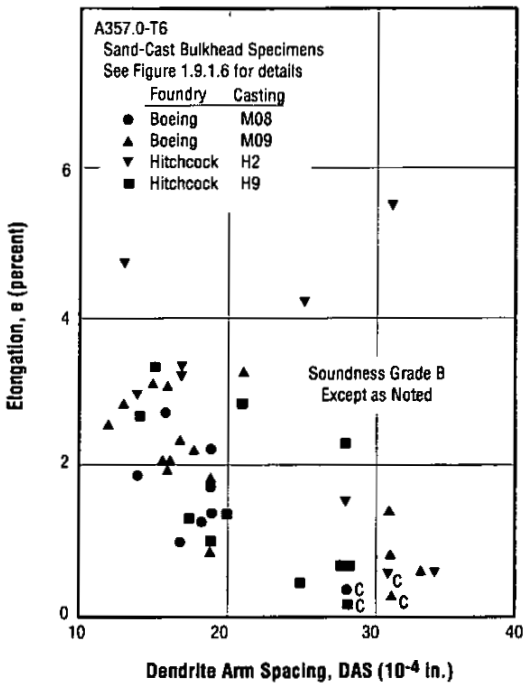

Figure 1.9.1.11 Effect of dendrite arm spacing on tensile elongation of specimens with Grades B and C soundness taken from sand-cast bulkheads (Ref. 10)

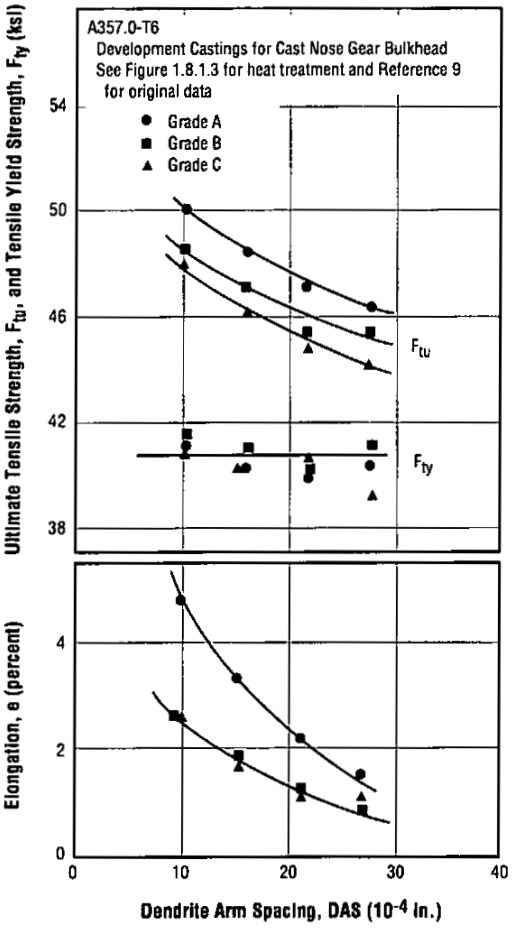

Figure 1.9.1.12 Effect of dendrite arm spacing and radiographic soundness on tensile properties of development castings (Ref. 16)

Note: The data shown represent the average of four selected DAS ranges. This subjective procedure greatly reduces the scatter in the original data.

Table 1.9.3.1 Effect of dross and gas porosity on tensile properties of shell investment and sand-cast plates (Ref. 12)

Alloy	A357.0-T6					
Form	Shell Investment Cast				Sand Casting	
Foundry Practice and Heat Treatment	See Table 3.2.1.4				See Table 3.2.1.5	
Type of Discontinuity	Dross		Gas Porosity		Dross	
Radiographic Grade[a]	A – B	C – D	A – B	C – D	A – B	C – D
F_{tu} (ksi)	49 – 51	42	49 – 51	33 – 38	51 – 53	31 – 47
F_{ty} (ksi)	40 – 42	40	40 – 42	31 – 38	43 – 45	30 – 42
e (percent)	4 – 5	0.5	4 – 5	0.5 – 2	6 – 9	0.2

[a] According to MIL-C-6021.

Table 1.9.3.2 Effect of excessive gas and shrinkage porosity on the tensile properties of sand castings (Ref. 12)

Alloy		A357.0-T6			
Form		Specially Cast Plates to Produce Low Quality Sand Casting			
Grade		D	C – D		B or Better[a]
Type of Discontinuity		Sponge Shrinkage	Round Gas Porosity		
ASTM Plate[b]		No. 4	No. 4	No. 7	
No. of Tests		3	3	2	106
F_{tu} (ksi)	Average	43.8	42.8	47.2	54.3
	Range	40.7 – 46.4	45.4 – 48.8	46.7 – 47.7	—
F_{ty} (ksi)	Average	41.3	42.3	41.3	45.8
	Range	39.7 – 42.2	41.8	42.7	—
e (percent)	Average	1.8	3	3	5.5
	Range	1 - 2	2 - 4	3 - 3	—

[a] See Table 3.2.1.2.

[b] ASTM E 155 Reference Radiographs.

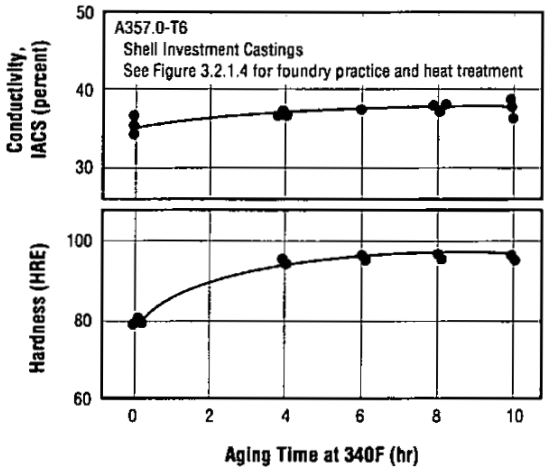

Figure 2.2.2.1 Effect of aging time on the electrical conductivity and hardness of shell investment castings (Ref. 12)

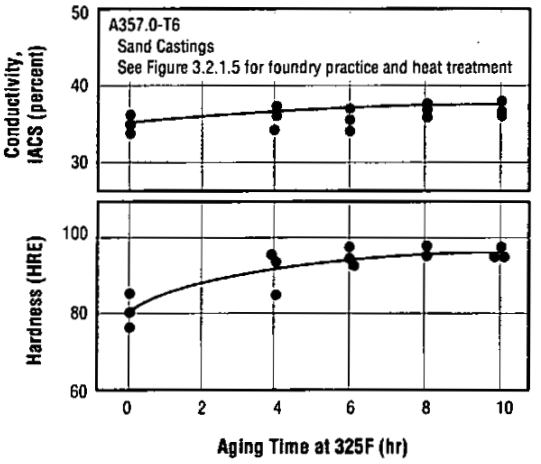

Figure 2.2.2.2 Effect of aging time on the electrical conductivity and hardness of sand castings (Ref. 12)

Table 3.1.1 AMS and ASTM specifications for mechanical properties and microstructure

Alloy	A357.0 and D357.0							
Specification[g]	AMS 4219	AMS 4219C	AMS 4249 and 4241A[c]		ASTM B 108		ASTM B 686	
Specimen Location	Any Area	Separately or Integrally Cast	Designated Area	Other Area	Separately Cast[f]	Designated Area[f]	Any Area	Designated Area
F_{tu} (ksi)	38	41	50	45	45	46	41	45
F_{ty} (ksi)	30	32	40	36	36	36	31	35
e (percent)	2	3	3	2	3	3	3	3
Hardness Brinell[d] 10 to 500kg 10 to 1000 Kg	85 to 115 85 to 120	85 to 115 85 to 120	90	90				

Special Requirements for AMS 4249[a,e]	
K_{Ic} (ksi $\sqrt{in.}$) ASTM E 1304	21
Fatigue Life[b] (cycles)	
Spec. Dia. = 0.5 in.	Log Avg. 85,000 Min. 46,000
Spec. Dia. = 0.375 in.	Log Avg. 78,000 Min. 42,000
Spec. Dia. = 0.25 in.	Log Avg. 88,000 Min. 36,000

[a] Each casting shall have at least two tensile and two fracture toughness coupons. One coupon to remain attached and used only if re-heat treatment is required.

[b] Three fatigue specimens (ASTM E 466) are to be tested from integrally cast coupons or from specimens cut from castings. Testing conditions are K_t = 1, Maximum Stress = 40 ksi, R = 0.1 and Frequency from 10 to 20 Hz. Specimens cut from castings may have gauge diameters of 0.5, 0.375 or 0.25 inches.

[c] The tensile properties shown above for AMS 4241A are associated with procedures for determining the dendrite arm spacing (DAS) from integrally cast chilled and unchilled specimens. These results are then used to determine the DAS necessary to achieve the specified properties. For details concerning DAS requirements reference should be made to AMS 4241A and its related documents.

[d] Casting should not be rejected on basis of hardness if tensile properties are met.

[e] Designated areas of castings shall have a DAS < 0.002 inch determined in accordance with ARP1947.

[f] Applies to castings with maximum section thickness of 2 inches.

[g] For references see Table 1.4.2.

Table 3.1.2 Military specification mechanical properties (Ref. 45)

Alloy	A357.0-T6 and D357.0-T6				
Source	MIL-A-21180D				
Specimen Location	Designated Areas		Any Area		
Strength Class	1	2	10	11	12
F_{tu} (ksi)	45	50	38	41	45
F_{ty} (ksi)	35	40	28	31	35
e (percent)	3	5	5	3	3

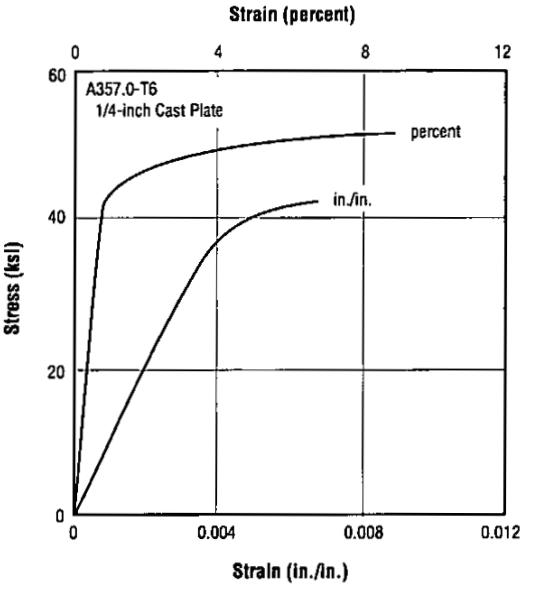

Figure 3.2.1.1 Stress-strain curves for sand-cast plate (Ref. 30)

Table 3.2.1.2 Tensile, compressive, shear, and bearing properties for specimens removed from designated areas of Northrop sand-cast stepped plates from Suppliers A and B (Ref. 12)

Alloy	A357.0-T6								
Condition	Specimens Taken From Northrop Sand-Cast Stepped Plates From Suppliers A and B (See Figure 1.8.1.1)								
Plate Area	Designated Areas (Radiographic Quality B or Better)[a]								
Property	F_{tu} (ksi)	F_{ty} (ksi)	e (percent)	F_{cy} (ksi)	F_{su} (ksi)	F_{bru}, 1.5 e/d (ksi)	F_{bry}, 1.5 e/d (ksi)	F_{bru}, 2.0 e/d (ksi)	F_{bry}, 2.0 e/d (ksi)
Number of Tests	106	106	106	106	10	10	10	10	10
Average	54.3	45.8	5.5	47.2	34.4	92.9	74.3	117.3	84.7
Standard Deviation	1.35	1.41	b	N/A	N/A	N/A	N/A	N/A	N/A
Low Value	51.7	42.2	2	44.1	33.7	90.6	69.4	107.5	82

[a] Includes designated and nondesignated areas from Supplier A since both areas had radiographic quality of B or better.

[b] Distribution not normal.

Note: N/A = not applicable (sample size too small for design purposes).

Table 3.2.1.3 Tensile, compressive, shear, and bearing properties for specimens removed from nondesignated areas of Northrop sand-cast stepped plates from Supplier B (Ref. 12)

Alloy	A357.0-T6								
Condition	Specimens Taken From Northrop Sand-Cast Stepped Plates From Supplier B (See Figure 1.8.1.1)								
Plate Area	Nondesignated Areas (Radiographic Quality B to C)								
Property	F_{tu} (ksi)	F_{ty} (ksi)	e (percent)	F_{cy} (ksi)	F_{su} (ksi)	F_{bru}, 1.5 e/d (ksi)	F_{bry}, 1.5 e/d (ksi)	F_{bru}, 2.0 e/d (ksi)	F_{bry}, 2.0 e/d (ksi)
Number of Tests	32	32	32	5	5	5	5	5	5
Average	50.5	43.7	3	45.6	33.8	92.4	74.8	116.4	82.6
Low Value	44.8	40.8	1	44.1	33.0	90.7	71.0	113.3	83.9

Table 3.2.1.4 Tensile properties and hardness of investment cast test plates (Ref. 12)

Alloy	A357.0-T6			
Form	3-inch x 10-inch x 3/16-inch Thick Shell Investment Casting			
Foundry Practice	300 lb Melt at 1300F + 1.4 lb (5% Ti + 1% B) Grain Refiner + (95% N + 5% Feron 12) Degas + 1300F Pressurized (3-1/2 psia) Pour + High-Pressure H_2O Clean			
Heat Treat	1000F 12 hr, WQ + 12 hr at RT + 340F 6 hr			
Tensile Properties	F_{tu} (ksi)	F_{ty} (ksi)	e (percent)	Hardness, RE
n = 10: $\bar{x}$	48.4	40.3	5.8	94
σ	0.88	0.60	1.08	1.43

Comments: Plate surface DAS range: 1.2 - 1.6 mils
Plate radiographic quality: Grade B (min)
One specimen per plate
10 plates, average Mg 0.51%, Fe 0.10 - 0.13%

Table 3.2.1.5 Tensile properties and hardness of sand-cast test plates (Ref. 12)

Alloy	A357.0-T6			
Form	3-inch x 10-inch x 3/16-inch Thick Shell-Cast Plates			
Foundry Practice	AFS Bank Sand With 0.8 percent Pepset Binder, Chills in Both Cope and Drag, Two Risers, Steel Wool and Screens in Well of Sprue, 1000-lb Melt at 1300F + (90% N + 10% Cl), Degas + 1375F, Pour			
Heat Treat	1010F 18 hr, 40F WQ (7-11 sec Q Delay) + 12-24 hr at RT + 325F 8 hr			
Tensile Properties	F_{tu} (ksi)	F_{ty} (ksi)	e (percent)	Hardness, RE
n = 9: $\bar{x}$	48.8	41.1	5.5	96
σ	0.89	1.02	0.90	0.87

Comments: Plate surface DAS range: 0.9 - 1.2 mils
Plate radiographic quality: Grade B (min)
One specimen per plate
9 plates, Mg 0.58 - 0.59%, Fe 0.08 - 0.12%

Table 3.2.1.6 Tensile properties of specimens removed from webs and flanges of a development casting for the F-16 vertical tailunderstructure (Ref. 13)

A357.0-T6
Development Sand Casting
See Table 3.2.1.7 for heat treatment

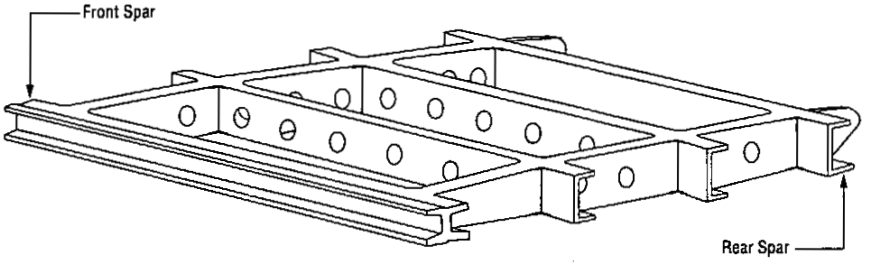

Casting		No. 2	No. 3
Number of Tests		20	20
F_{tu} (ksi)	Average	50.8	51.0
	Range	45.4 – 53.6	47.8 – 53.5
F_{ty} (ksi)	Average	39.4	39.2
	Range	36.8 – 42.3	36.7 – 43.3
e (percent)	Average	9.6	10.7
	Range	5 – 17	7 – 15

Table 3.2.1.7 Tensile properties of composite sand-cast F-16 vertical tail understructure cast at Alcoa (Ref. 13)

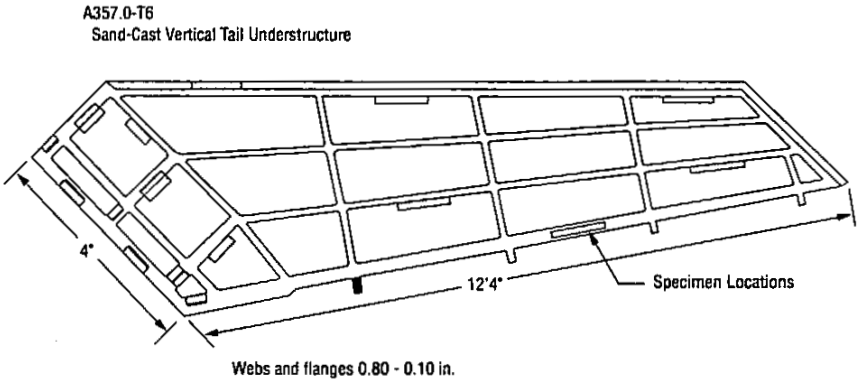

Foundry Practice	Melt in Two 500-lb Silicon Carbide Crucibles at 1300F, Degas with 90% N_2 + 10% Cl_2 for 20 min, Vacuum Gas Check (2 - 5 mm Hg With No Bubbles Permitted).Raise Melt to 1440F and Add 5% Ti + 1% B as Grain Refiner. Pour at 1440F. Solution Treat 1010F 15 hr, Quench in 15% Ucon A + Water, Hold 16 hr at RT, Age 310F 6 hr					
Casting Number	2	3	5	6	7	8
Number of Specimens	25	26	29	32	9	8
F_{tu} (ksi) Mean	50.8	50.8	49.0	48.7	51.4	52.2
Std Dev	1.86	1.55	2.38	3.50	0.95	0.74
F_{ty} (ksi) Mean	39.2	40.3	38.6	39.2	38.1	40.6
Std Dev	1.31	3.53	1.27	1.83	0.85	0.65
e (percent) Mean	9.5	10.1	9.3	7.3	13.5	11.1
Std Dev	2.71	2.40	3.32	4.06	1.93	2.23
Results From All Six Castings						
F_{tu} (ksi) Average 49.9 Range 42.3[a] – 53.6	F_{ty} (ksi) Average 39.0 Range 35.5 – 43.3		e (percent) Average 9.4 Range 2[a] – 17.0			

[a] Specimen not machined all over.

Table 3.2.1.8 Average tensile properties of specimens removed from two full-scale bulkheads from the Boeing Foundry (Ref. 10)

Alloy	A357.0-T6					
Foundry	Boeing					
Casting	M08			M09		
Location[a]	F_{tu} (ksi)	F_{ty} (ksi)	e (percent)	F_{tu} (ksi)	F_{ty} (ksi)	e (percent)
Lugs	52.6	42.6	6.1	51	41.1	5.4
Upper Flange	48.2	39.5	3.1	46.9	38.5	2.7
Corrugations	49.1	40.6	2.0	47.4	39.8	3.0
Webs and Stiffeners	49.7	42.7	2.1	46.7	40.8	1.7
Fitting	50.3	43.0	2.2	50.5	41.2	4.5
Periphery Flange	45.0	41.9	0.6	44.8	40.9	1.0

[a] For locations and heat treatments, see Figure 1.8.1.3.

Table 3.2.1.9 Average tensile properties of specimens removed from two full-scale bulkheads from the Hitchcock Foundry (Ref. 10)

Alloy	A357.0-T6					
Foundry	Hitchcock					
Casting	H2			H9		
Location[a]	F_{tu} (ksi)	F_{ty} (ksi)	e (percent)	F_{tu} (ksi)	F_{ty} (ksi)	e (percent)
Lugs	49.4	38.1	7.7	48.1	38.1	5.1
Upper Flange	45.3	34.5	4.7	44.4	34.9	2.7
Corrugations	47.0	38.6	3.7	45.5	38.5	2.1
Webs and Stiffeners	46.8	39.1	2.8	45.9	39.1	2.3
Fitting	48.4	39.9	3.6	46.4	39.4	2.0
Periphery Flange	44.8	41.8	0.6	42.6	41.2	0.4

[a] For locations and heat treatments, see Figure 1.8.1.3.

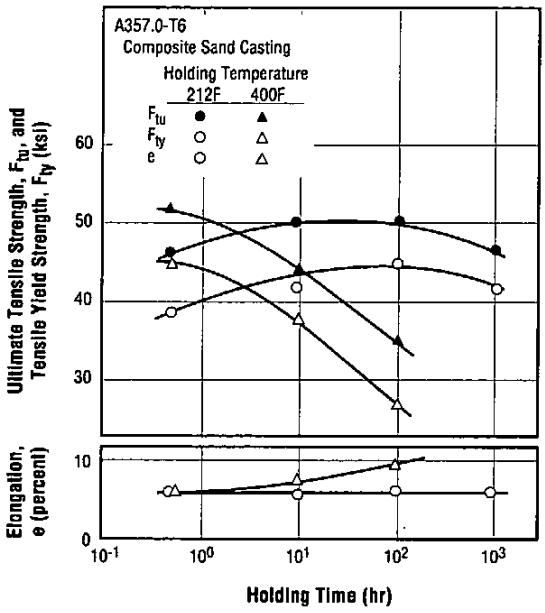

Figure 3.2.1.10 Effect of holding time at 212 or 400F on tensile properties at room temperature (Ref. 19)

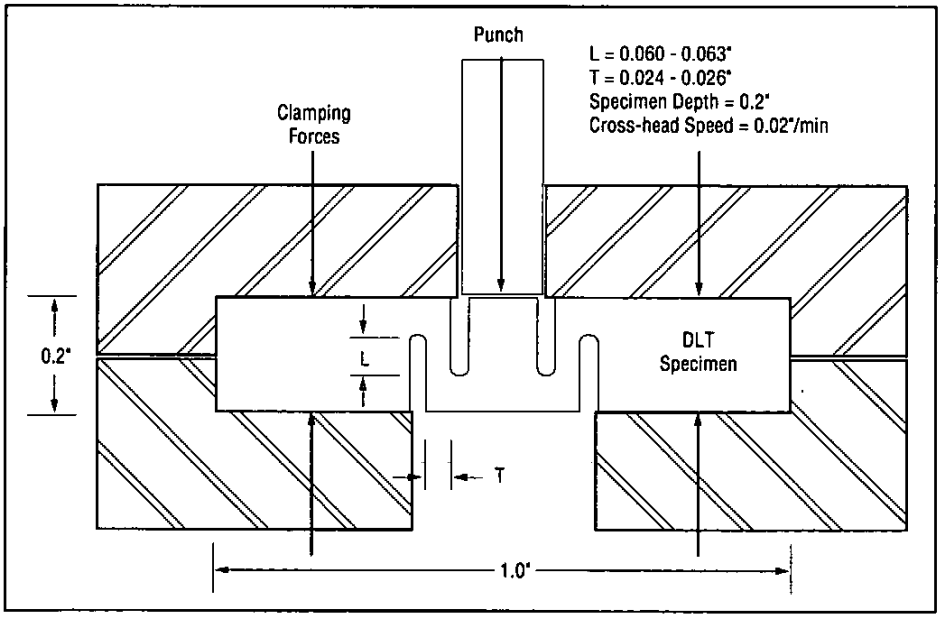

Figure 3.2.1.11 Configuration of double ligament tensile (DLT) specimen in test rig used to measure anisotropy in mechanical properties of cylindrical sand castings (Ref. 42)

Table 3.2.1.12 Effect on tensile properties of specimen orientation with respect to axis of sand-cast cylinders (Ref. 42)

Alloy	A357.0-T6		
Form	Sand-Cast Cylinders 6-inch outside diameter, 1-inch inside diameter		
Composition	7.0 Si, 0.08 Fe, 0.20 Cu, 0.55 Mg, 0.10 Zn, 0.05 Be		
Specimen Geometry	DLT (See Figure 3.2.1.11 for details)		
Test Conditions	RT, Laboratory Air, 55% R.H		
Ligament Orientation With Respect to Axis of Cylinder[a]	F_{ty} (ksi)	F_{tu} (ksi)	e (percent)
Longitudinal	42.9	54.6	8.9
Radial	41.3	55.0	9.6
Tangential	42.4	50.1	8.0

[a] Average of four tests per orientation.

Table 3.2.1.13 Smooth tensile, notch tensile and fracture toughness properties of specimens from sand composite cast plates from three suppliers and from F5 wing pylons (Ref. 41)

Alloy	D357.0-T6							
Composition	AMS 4241 plus Si modifier (either Sr or Na)							
Form	16 x 6 x 1.25-in. cast plates from three foundries, each using metal chills in somewhat different rigging						F5 wing pylon 65 lb; 5' long	
Supplier	Foundry A		Foundry B		Foundry C		Alcoa	
Si Modifier	Na		Sr		Na		See below	
Solution Treat	1015F 15 hr RT WQ or RT GQ[a]		1010F 24 hr RT WQ or RT GQ		1010F 19 hr RT WQ or 1010F 16 hr, RT GQ		1010F 15 hr RT WQ	
Age	335F 6 hr		315F 13 hr		RT 24 hr, 335F 6 hr		325F 5.5 hr	
Properties	Water Quench	Glycol Quench	Water Quench	Glycol Quench	Water Quench[b]	Glycol Quench[b]	Na mod.	Sr mod.
F_{tu}[c] (ksi)								
Average	54	53	52	49	54	51	52	53
Minimum	51	51	50	48	53	50	49	49
Maximum	55	55	53	50	55	52	53	53
F_{ty} (ksi)								
Average	45	43	45	42	47	44	42	41
Minimum	44	42	44	41	46	43	39	39
Maximum	47	44	46	43	48	44	44	43
e (percent)								
Average	5.9	6.6	4.5	3.4	5.4	4.9	6.8	10.2
Minimum	3.5	5.5	3.0	2.5	3.9	4.6	3.5	8.0
Maximum	8.5	9.0	5.6	4.3	8.2	5.2	8.6	11.7
NTS/F_{ty}[d]								
Average	1.40	1.33	1.36	1.38	1.12	1.01	1.44	1.49
Minimum	1.23	1.30	1.30	1.35	0.97	0.98	1.44	1.49
Maximum	1.51	1.36	1.45	1.41	1.36	1.07	1.44	1.49
K_{Ic}[e] (ksi $\sqrt{in.}$)								
Average		21		22		22		

[a] 25 percent glycol solution.

[b] Second batch of cast plates; first batch rejected for low elongation.

[c] ASTM B 557 specimen.

[d] ASTM E 602 0.5-inch D specimen.

[e] ASTM B 647 compact tension specimen.

Table 3.2.1.14 Smooth tensile and fracture toughness properties of specimens from sand composite cast plates with intentional defects (Ref. 41)

Alloy	D357.0-T6								
Composition	AMS 4241 plus Si modifier (Na)								
Form	16 x 6 x 1.25-in. Cast Plates								
Supplier	Alcoa								
Si Modifier	Na								
Solution Treat	1015F 15 hr, RT WQ or RT GQ[a]								
Age	335F 6 hr								
Properties	Baseline[b]	Gas Porosity			Shrinkage Porosity		Foreign Material		Weld Repair[e]
	Grade A/B	Grade B	Grade C	Grade D	Grade B	Grade C	Grade B	Grade C	Grade A/B
F_{tu}[c] (ksi)									
Average	54	51	50	49	51	51	54	53	55
Minimum	53	47	49	48	50	50	51	49	54
Maximum	55	52	53	49	53	51	55	53	56
F_{ty} (ksi)									
Average	48	45	46	44	46	46	46	41	47
Minimum	47	42	44	44	44	45	45	39	46
Maximum	48	46	48	45	48	46	48	43	48
e (percent)									
Average	3.9	3.3	2.7	1.5	2.7	2.9	4.6	10.2	5.1
Minimum	1.1	2.1	1.5	1.3	1.5	2.2	3.1	8.0	3.5
Maximum	5.0	4.3	7.9	1.7	7.9	3.9	7.5	11.7	8.0
K_{Ic}[d] (ksi $\sqrt{in.}$)									
Average		21	22		20	23			

[a] 25 percent glycol solution.

[b] No intentional defects.

[c] ASTM B 557 specimen.

[d] ASTM E 602 compact tension specimen.

[e] See Section 4.3.1.1 for description of tests.

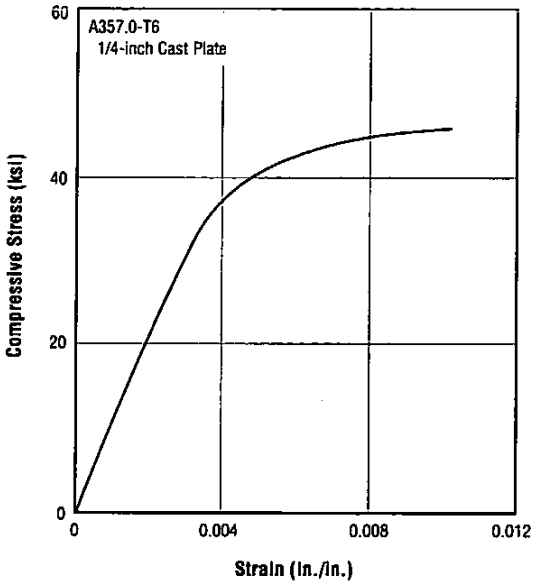

Figure 3.2.2.1 Compressive stress-strain curve for sand-cast plate (Ref. 30)

Table 3.2.7.2.2 Results of tests on ASTM E 399 compact specimens removed from separately sand-cast blocks (Ref. 31)

Alloy	A357.0-T6											
Form	0.690 - 0.750-inch Thick CT Specimens From Separately Cast Blocks (See Figure 1.8.1.3 for Heat Treatment)											
F_{ty} (ksi)	41	41	40	42	42	41	41	36	42	42	38	38
K_Q[a] (ksi $\sqrt{in.}$)	20.5	11.6	17.5	14.3	—	13.5	—	17.2	—	20.8	—	19.9
K_{Ic}[b] (ksi $\sqrt{in.}$)	—	—	—	—	16.6	—	16	—	19.4	—	18.2	—

[a] Values not valid due to excessive crack front curvature.

[b] Values valid according to ASTM E 399-78.

Table 3.2.7.2.3 Results of tests on ASTM E 399 compact specimens removed from sand-cast bulkhead lugs (Ref. 7)

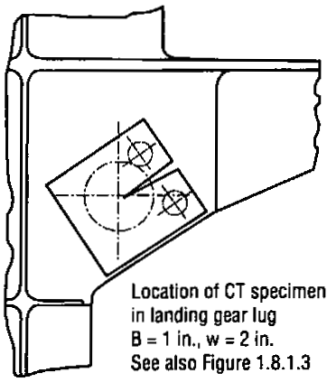

Supplier A	Supplier B
K_Q[a] (ksi $\sqrt{in.}$)	K_Q[a] (ksi $\sqrt{in.}$)
24.4	21.6
20.5	20.8
20.6	19.7
20.0	20.6
21.4	18.3 } [b]
21.6	18.7 } [b]
	13.9 } [b]

[a] No valid K_{Ic} values due to crack curvature.

[b] Excessive microshrinkage.

Table 3.2.7.2.4 Results of tests on ASTM E 399 compact specimens removed from separately sand-cast blocks and from designated areas of stepped plates (Ref. 12)

Alloy	A357.0-T6		
Foundry Practice and Heat Treatment	See Table 3.2.1.5		See Figure 1.8.1.1
Form	Separately Cast Block		Stepped Plates Designated Areas
Supplier	A	B	A
F_{tu} (ksi)	51.4	52.3	55
F_{ty} (ksi)	43.3	45.9	47.2
e (percent)	6	5	7.7
Specimen Thickness (in.)	0.8	0.8	0.5
K_Q[a] (ksi $\sqrt{in.}$) Range	25.7 - 26.7	25.5 - 26.6	18.5 - 25.2

[a] No valid E 399 values due to insufficient thickness or excess crack curvature.

Table 3.2.7.2.5 Results of tests on ASTM E 399 compact specimens removed from full-scale F-16 vertical tail understructure (Ref. 13)

Alloy	A357.0-T6	
Form	CT Specimens From Full-Scale F-16 Vertical Tail Understructure (See Table 3.2.1.7)	
Specimen No.	Thickness (in)	K_Q[a] (ksi $\sqrt{in.}$)
2	0.295	23.1
5	0.154	25.8
7	0.293	22.7
10	0.248	30.1

[a] Insufficient thickness according to ASTM E 399.

Table 3.2.7.2.6 Fracture toughness of specimens removed from intentionally produced defective step plates (Ref. 12)

Alloy	D357.0
Castings	Step Plates (See Figure 1.8.1.1)
Radiographic Grade	Worse than D
Discontinuity Type	Sponge Shrinkage Nos. 6 and 7
Specimen	0.5-in thick CT
K_Q (ksi $\sqrt{in.}$)	
Minimum	22.5
Maximum	25.1
Average	23.0
Number of Tests	3

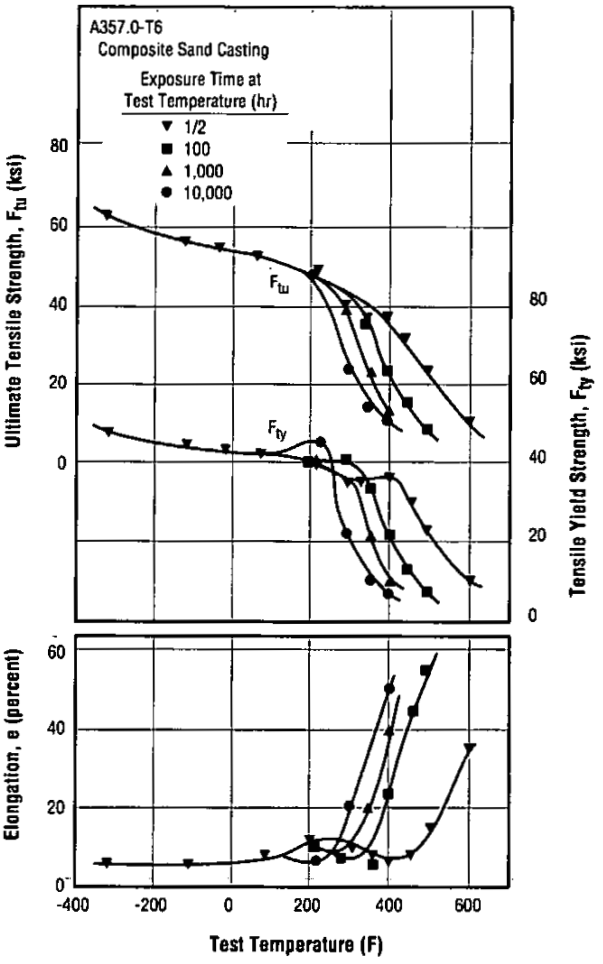

Figure 3.3.1.1 Effect of test temperature and holding time on tensile properties (Ref. 19)

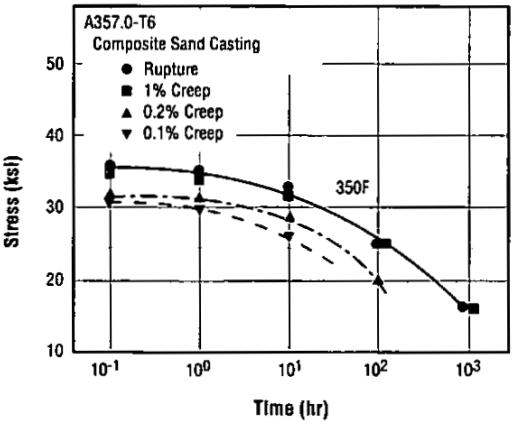

Figure 3.4.1 Creep and creep rupture at 350F (Ref. 19)

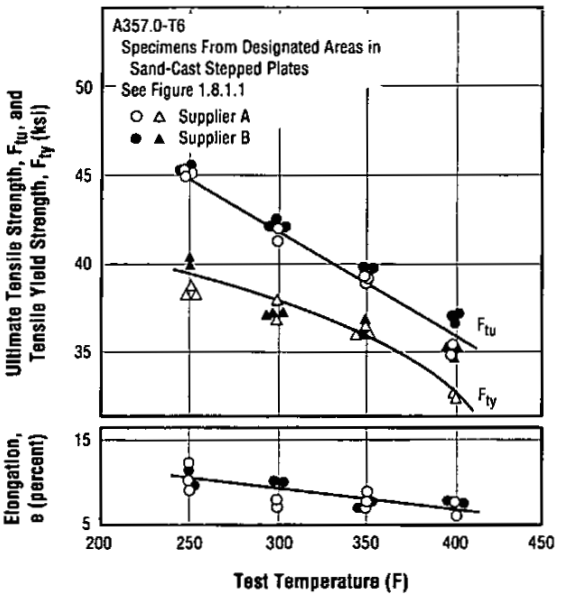

Figure 3.3.1.2 Effect of elevated test temperature on tensile properties of sand castings (Ref. 12)

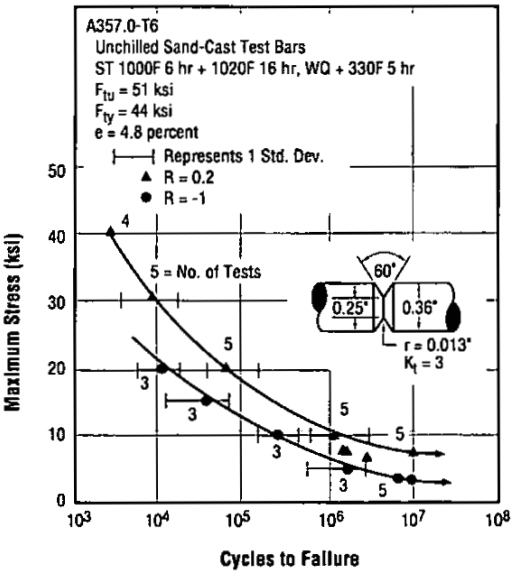

Figure 3.5.1.1 S-N curves for axial fatigue of separately sand-cast test specimens (Ref. 17)

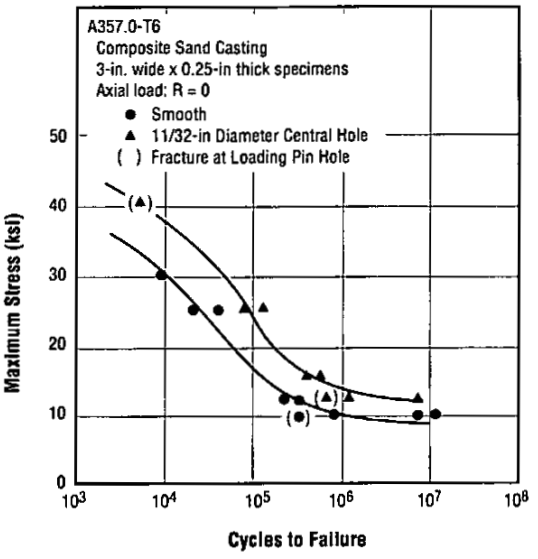

Figure 3.5.1.2 S-N curves for smooth and notched specimens (Ref. 19)

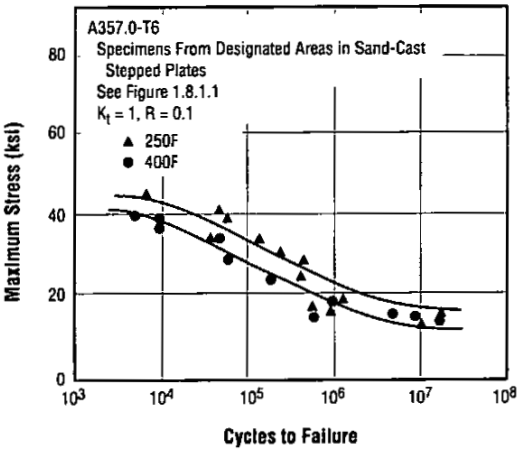

Figure 3.5.1.3 S-N curves at elevated tempertures for specimens removed from sand-cast stepped plates (Ref. 32)

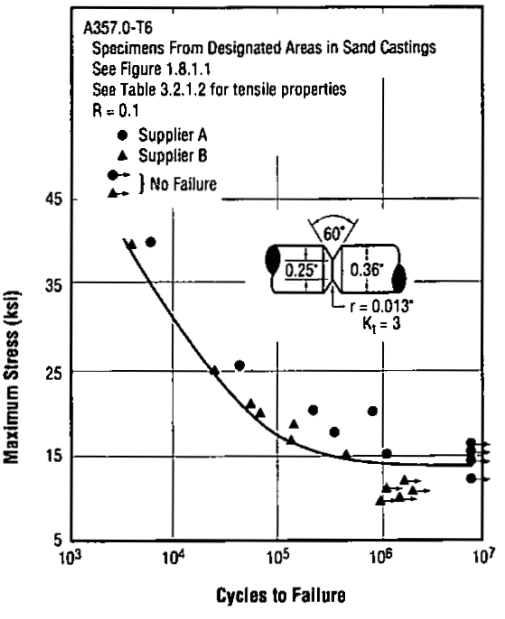

Figure 3.5.1.4 S-N curves for notched specimens from sand-castings (Ref. 12)

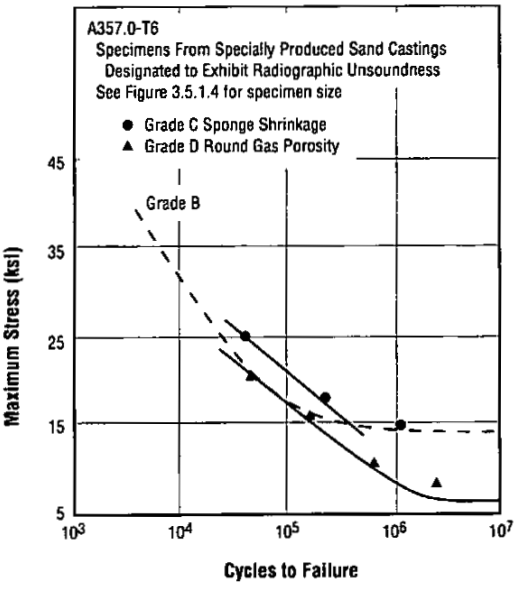

Figure 3.5.1.5 Effect of sponge shrinkage (Grade C) and round gas porosity (Grade D) on notched fatigue properties of sand castings (Ref. 12)

Table 3.5.1.6 Smooth and notched fatigue properties of separately sand-cast specimens and specimens removed from cast bulkhead (Refs. 4, 7)

Alloy	A357.0-T6 Sand-Cast		
Condition	Separately Cast Specimens (4)		Specimens From Bulkhead Corrugations (7)
Specimen Type[a]	Smooth	$K_t = 3$	$K_t = 3$
Number of Tests	20	16	10
Maximum Stress (ksi), R = 0.06	18	16	18
Range of Cycles to Failure (10^3)	75 - 380	58 - 180	30 - 103
Weibull Characteristic Life (10^3 cycles)	220	98	—
95 percent Reliability With 95 percent Confidence (Weibull) Cycles to Failure (10^3)	56	26	—

[a] Specimens approximately 1-1/8 inch wide by 1/8 inch thick. $K_t = 3$; specimens had 3/16-inch diameter hole.

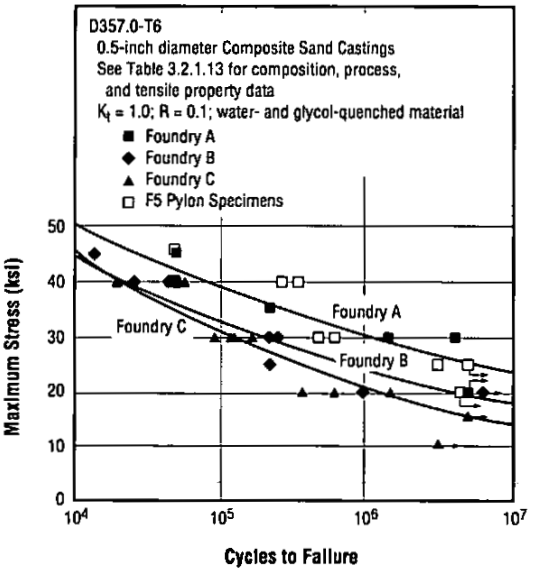

Figure 3.5.1.7 S-N curves for smooth specimens from composite sand-cast plates from three suppliers and from designated areas of four F5 wing pylons (Ref. 41)

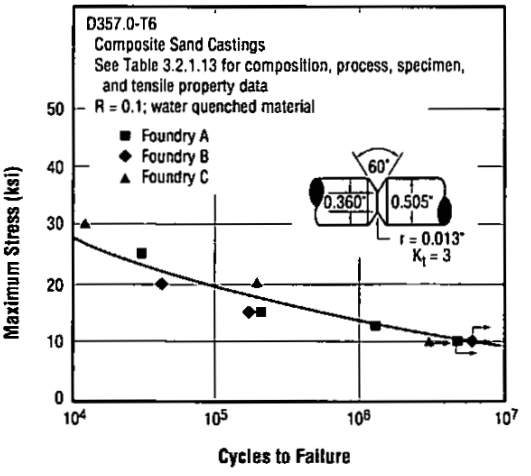

Figure 3.5.1.8 S-N curves for notched specimens from composite sand-cast plates from three suppliers (Ref. 41)

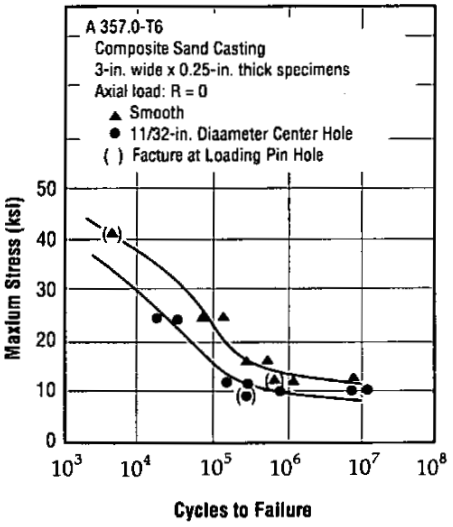

Figure 3.5.1.2 S-N curves for smooth and notched specimens (Ref. 19).

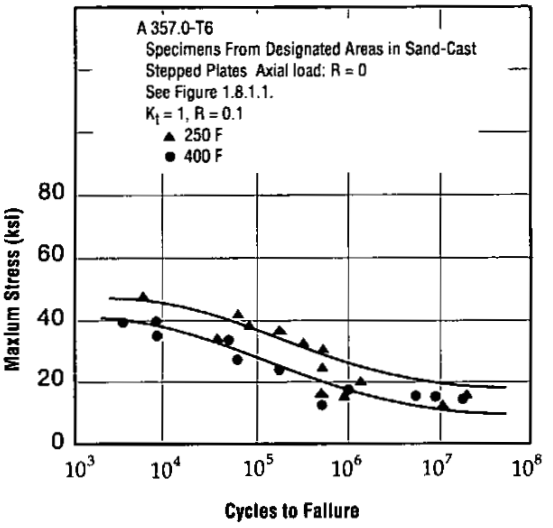

Figure 3.5.1.3 S-N curves at elevated temperatures for speciment removed from sand-cast stepped plates (Ref. 32)

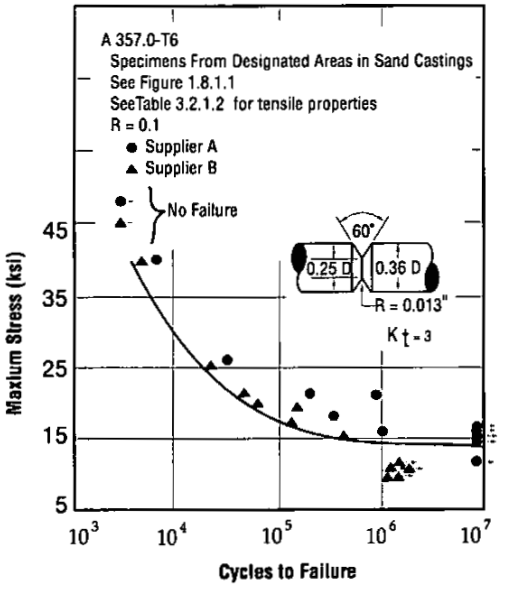

Figure 3.5.1.4 S-N curves for notched specimens from sand-castings (Ref. 12)

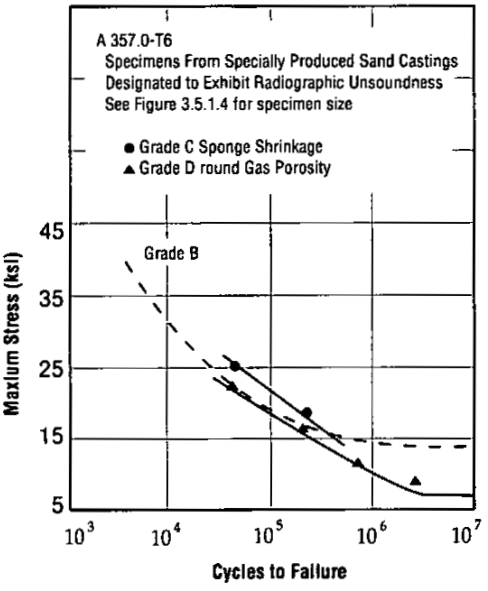

Figure 3.5.1.5 Effect of sponge shrinkage (Grade C) and round gas porosity (Grade D) on notched fatiguw properties of send castings (Ref. 12)

Table 3.5.1.6. Smooth and notched fatigue properties of separately sand-cast specimens and specimens removed from cast bulkhead (Refs. 4, 7)

Alloy	A357.0-T6 Sand-Cast		
Condition	Separately Cast Specimens (4)		Specimens from Bulkhead Corrugation (7)
Specimen Type[a]	Smooth	$K_t = 3$	$K_t = 3$
Number of Tests	20	16	10
Maximum Stress (ksi), R = 0.06	18	16	18
Range of Cycles to Failure (10^3)	75-380	58-180	30-103
Weibull Chaaracteristic Life (10^3 cycles)	220	98	–
95 percent reliability with 95 percent confidence (Weibull Cycles to Failure (10^3)	56	26	–

[a] Specimens approximaately 1-1/8 inch wide by 1/8 inch thick $K_t = 3$; specimens had 3/16-inch diameter hole.

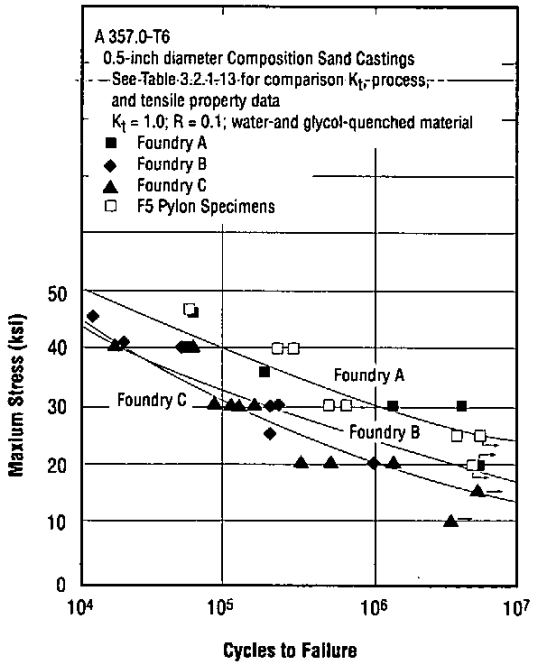

Figure 3.5.1.7 S-N curves for smooth specimens from composite sand-cast plates from three suppliers and from designated areas of four F5 wing Pylons (Ref. 41)

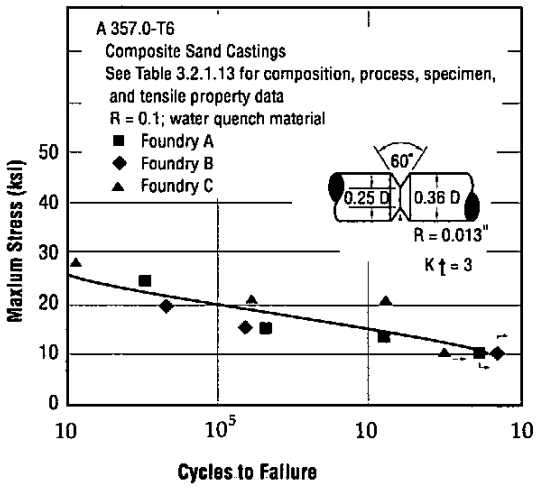

Figure 3.5.1.8 S-N curves for notched specimens from composite sand-cast plates from three suppliers (Ref. 41)

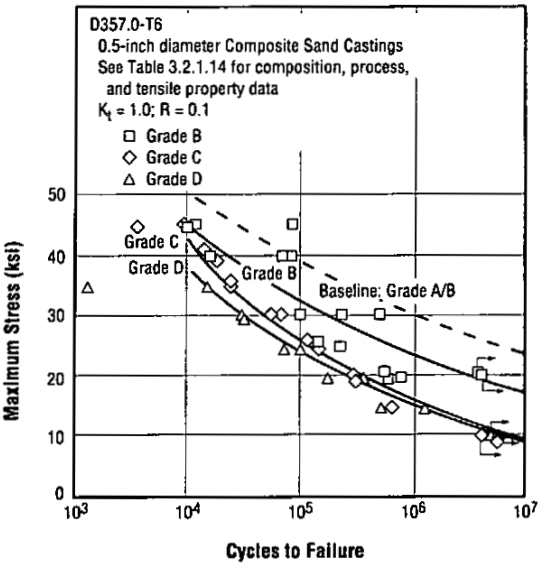

Figure 3.5.1.9 Effect of gas porosity on S-N curves for smooth specimens from composite sand-cast plates (Ref. 41)

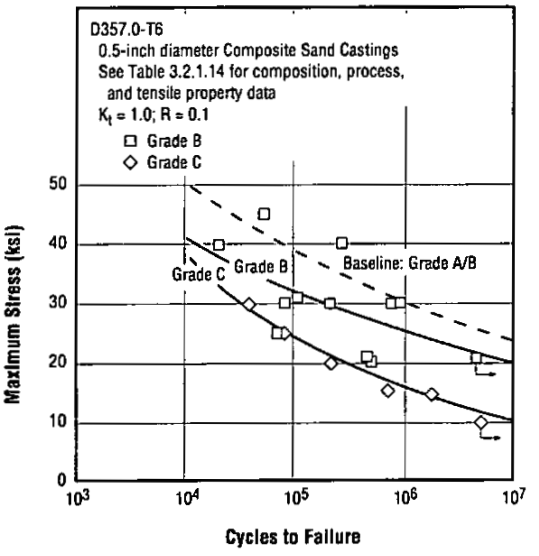

Figure 3.5.1.10 Effect of shrinkage porosity on S-N curves for smooth specimens from composite sand-cast plates (Ref. 41)

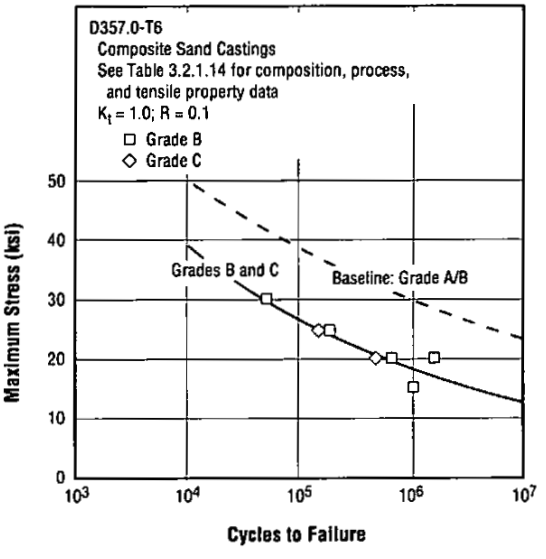

Figure 3.5.1.11 Effect of dross on S-N curves for smooth specimens from composite sand-cast plates (Ref. 41)

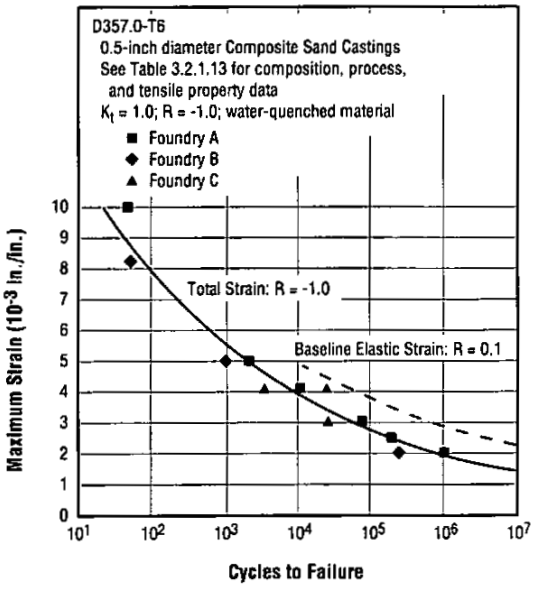

Figure 3.5.2.1 Strain-fatigue life curve for smooth specimens from composite sand-cast plates from three suppliers (Ref. 41)

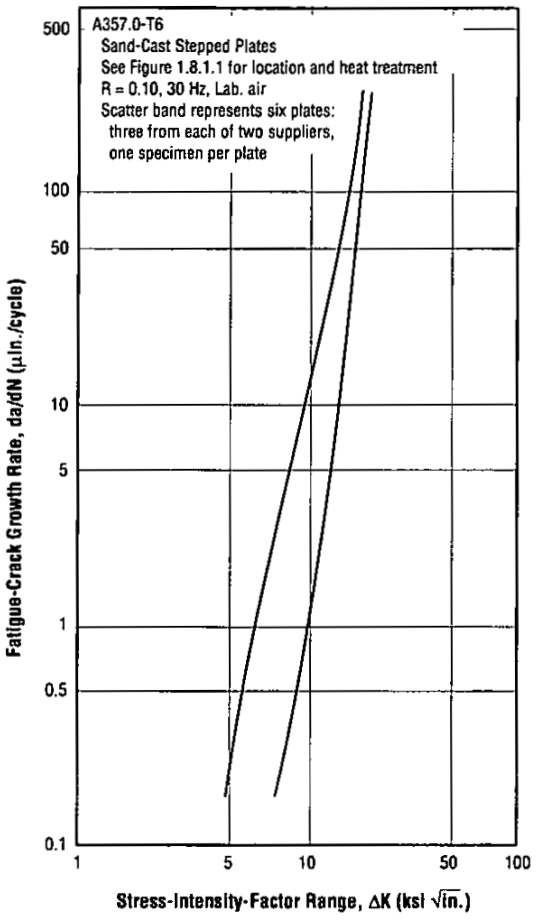

Figure 3.5.3.1 Fatigue-crack growth rates for specimens removed from designated areas in sand-cast stepped plates (Ref. 12)

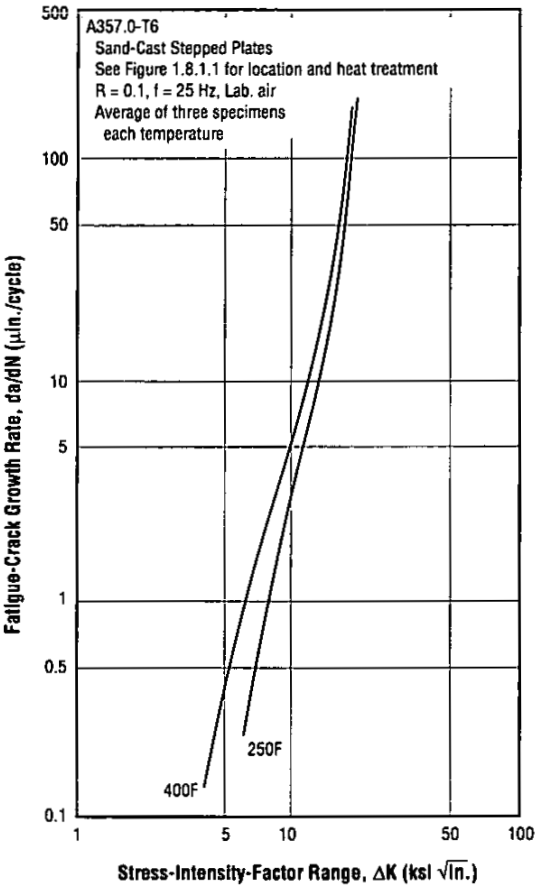

Figure 3.5.3.2 Fatigue-crack growth rates at 250 and 400F for specimens removed from designated areas in sand-cast stepped plates (Ref. 12)

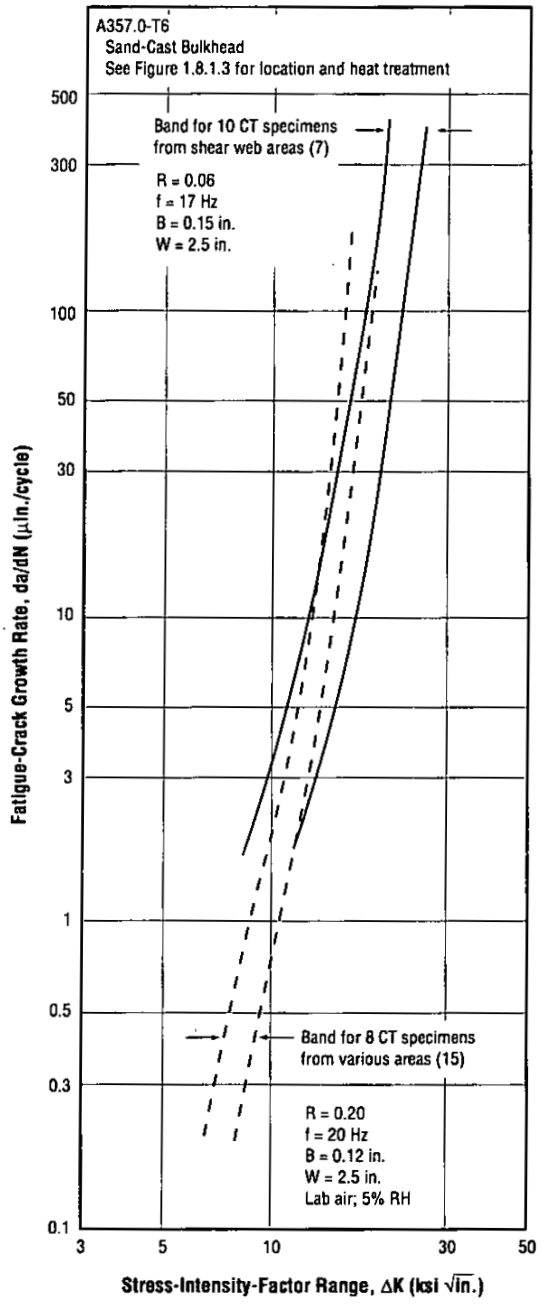

Figure 3.5.3.3 Scatter bands of fatigue-crack growth rates for specimens removed from a cast bulkhead (Refs. 7, 15)

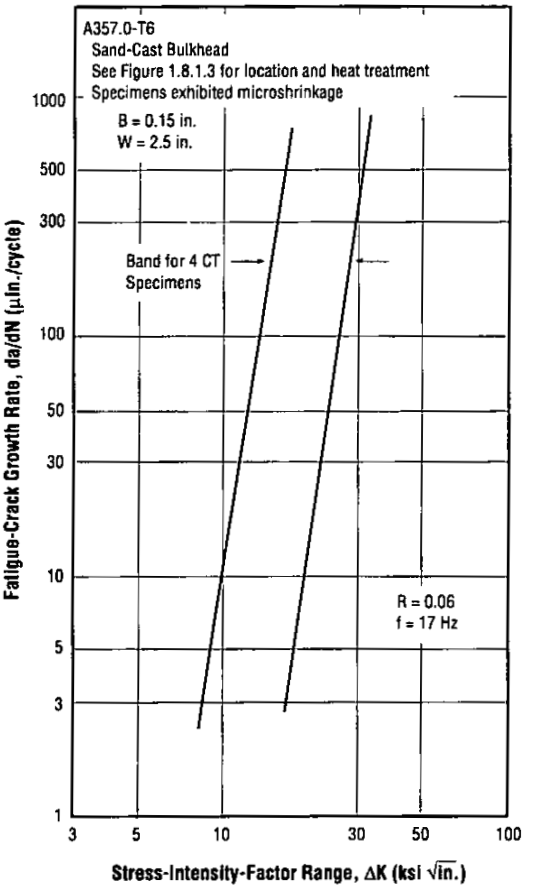

Figure 3.5.3.4 Scatter band of fatigue-crack growth rates for specimens removed from a cast bulkhead in shear web areas exhibiting microshrinkage (Ref. 7)

Table 3.5.3.5 Measures of the variability in cycles required to grow a crack from an initial to a final value (derived from tests on seven specimens) (Ref. 15)

Alloy	A357.0-T6			
Form	Cast Full-Scale Bulkheads (see Figure 1.8.1.3 for details)[a]			
Test Condition	a_f Constant			
a_i (in.)	a_f (in.)	Mean Life (kcycles)	Std Dev of Life	C.O.V.[b]
0.688	1.302	828.2	143.0	0.18
0.749	—	595.3	95.9	0.16
0.841	—	303.6	69.8	0.23
0.933	—	131.2	26.7	0.20
1.026	—	46.83	4.3	0.09
1.118	—	12.75	3.4	0.26
1.120	1.302	2.2	1.26	0.57
Test Condition	$(a_i - a_f)$ Constant			
0.688	0.749	232.9	56.3	0.24
0.749	0.841	290.5	55.2	0.19
0.841	0.933	173.3	45.4	0.26
0.933	1.026	84.38	23.6	0.28
1.026	1.118	34.04	4.55	0.13
1.118	1.210	10.54	2.4	0.23
1.120	1.302	2.21	1.3	0.57

[a] Average tensile properties from specimens cut from fatigue-crack growth CT specimens: F_{tu} = 49.9 ksi, F_{ty} = 43.5 ksi, e = 4.3 percent.

[b] Coefficient of variation.

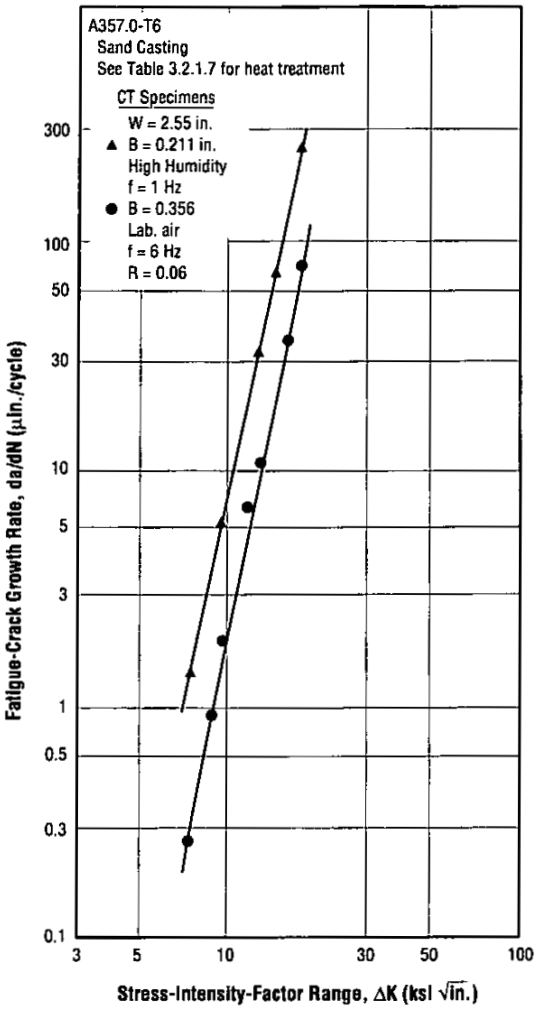

Figure 3.5.3.6 Fatigue-crack growth rates in lab air and in high humidity for specimens removed from full-scale F-16 vertical tail substructure (Ref. 13)

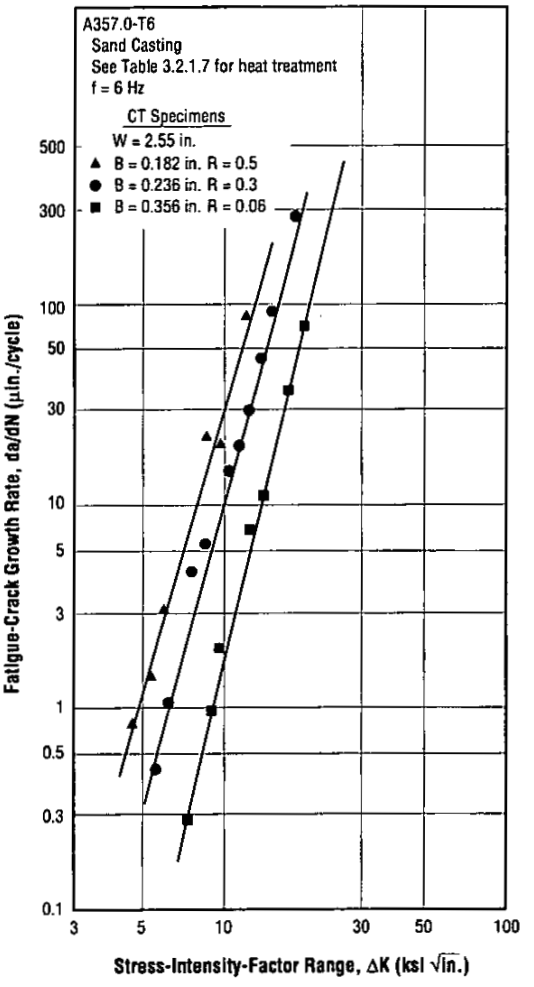

Figure 3.5.3.7 Fatigue-crack growth rates at several R-ratios for specimens removed from full-scale F-16 vertical tail substructure (Ref. 13)

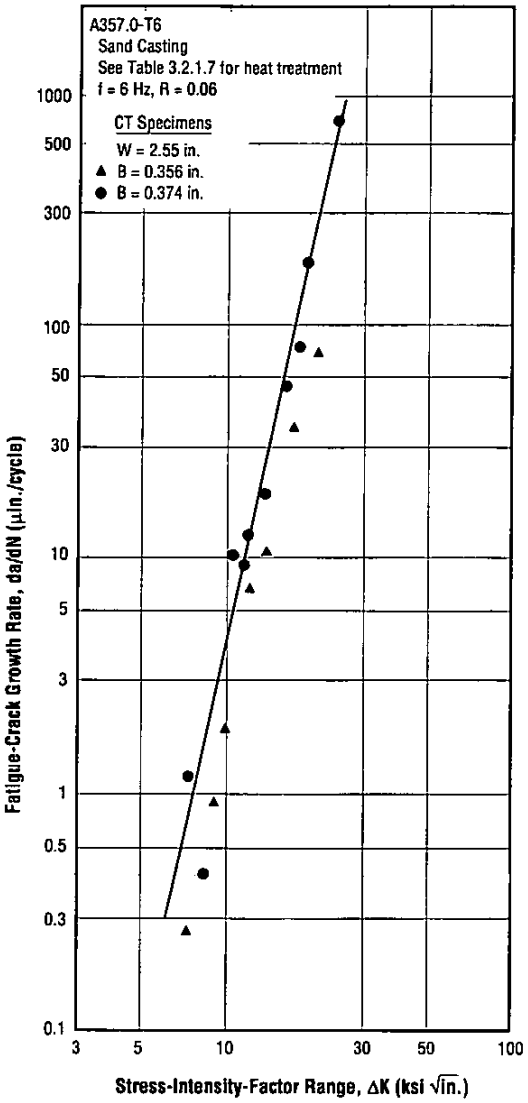

Figure 3.5.3.8 Fatigue-crack growth rates for specimens removed from full-scale F-16 vertical tail substructure (Ref. 13)

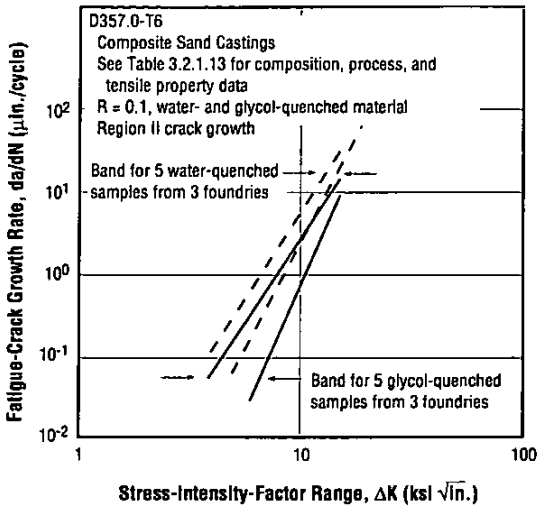

Figure 3.5.3.9 Scatter bands of fatigue-crack growth rates for specimens from composite sand-cast plates from three suppliers, for water- and glycol-quenched conditions (Ref. 41)

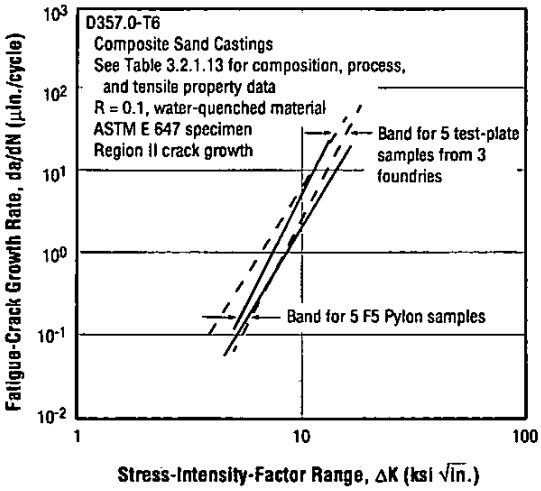

Figure 3.5.3.10 Scatter bands of fatigue-crack growth rates for specimens cut from a F5 aircraft wing pylon, compared with plate specimen growth rates (Ref. 41)

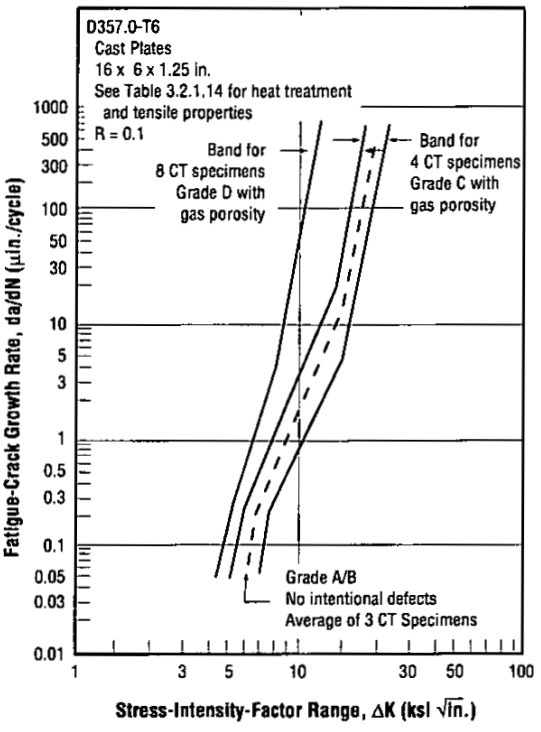

Figure 3.5.3.11 Effects of gas porosity on fatigue-crack growth rates of specimens from cast plates (Ref. 41)

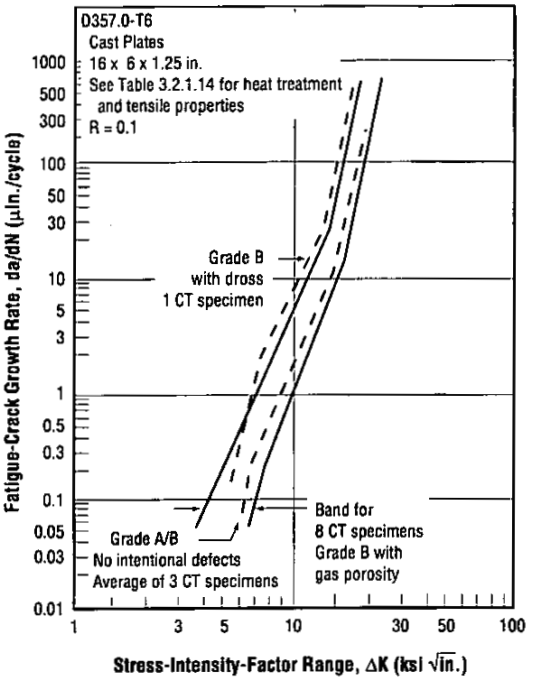

Figure 3.5.3.12 Effects of gas porosity or dross on fatigue-crack growth rates of specimens from cast plates (Ref. 41)

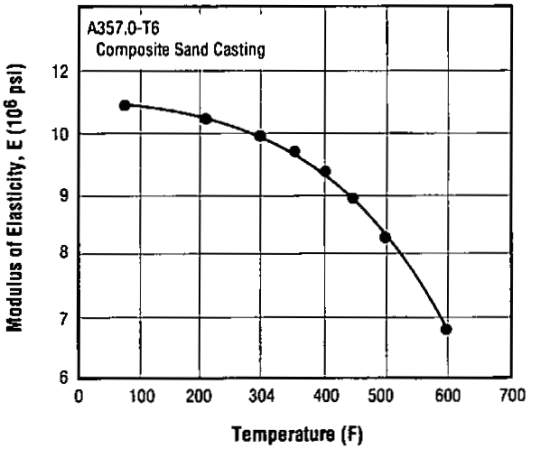

Figure 3.6.2.1 Effect of temperature on tensile modulus of elasticity (Ref. 20)

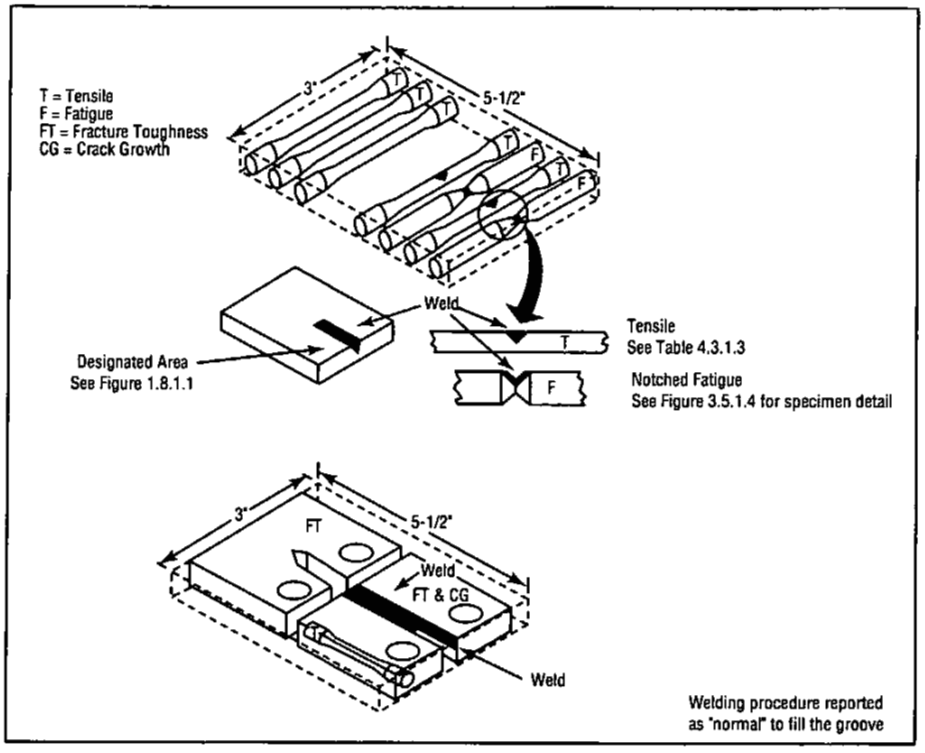

Figure 4.3.1.2 V-grooved (60-degree V, 0.25-inch deep with 3/32-inch radius) weld specimens from Northrop stepped plates (Ref. 12)

Table 4.3.1.3 Effect of weld repairs on tensile properties and fracture toughness of specimens from stepped plate sand castings (Ref. 12)

Alloy	A357.0-T6 Sand Castings							
Condition	V-Grooved Welds in Designated Areas of Northrop Stepped Plates (See Figure 4.3.1.2 for Configuration)							
Test Type	Tensile						Fracture Toughness[b]	
Welded	Yes			No			Yes	No
	F_{tu} (ksi)	F_{ty} (ksi)	e (percent)	F_{tu} (ksi)	F_{ty} (ksi)	e (percent)	K_Q (ksi $\sqrt{in.}$)	K_Q (ksi $\sqrt{in.}$)
Average	55.5	46.0	7.7	55.0	47.2	7.7	24.2	21.5
Range[a]	54.4 - 56.4	45.0 - 47.5	5.0 - 9.0	—	—	—	22.8 - 27.4	18.5 - 25.2

[a] Six tensile and three fracture toughness specimens per condition.

[b] Compact specimens approximately 0.5 inch thick; insufficient to yield valid ASTM E 399 values.

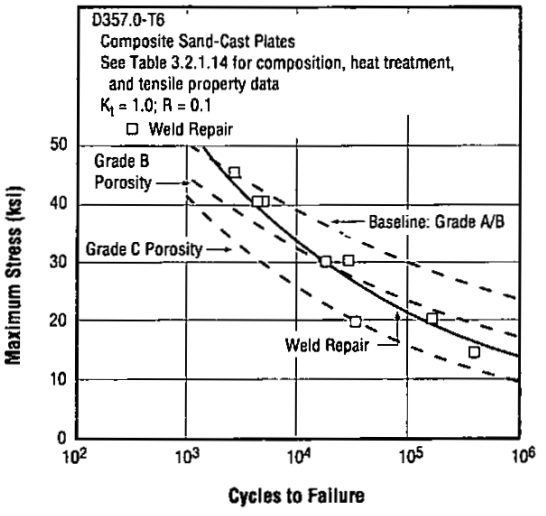

Figure 4.3.1.4 Effect of weld repairs on fatigue strength of smooth specimens from composite sand-cast stepped plates, compared with effects of gas porosity alone (Ref. 41)

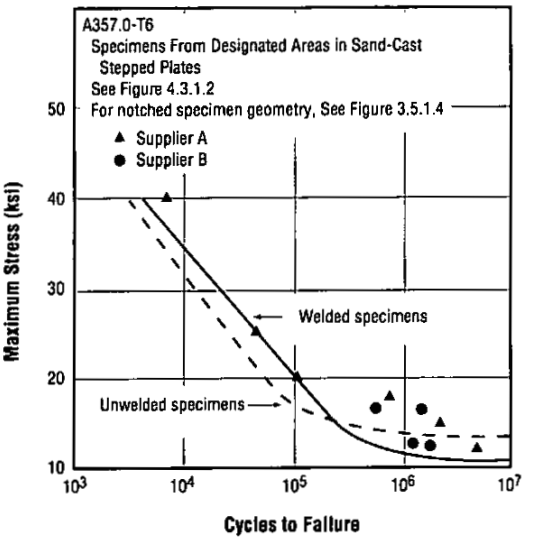

Figure 4.3.1.5 Effect of weld repairs on fatigue strength of notched specimens from stepped plate composite sand castings (Ref. 12)

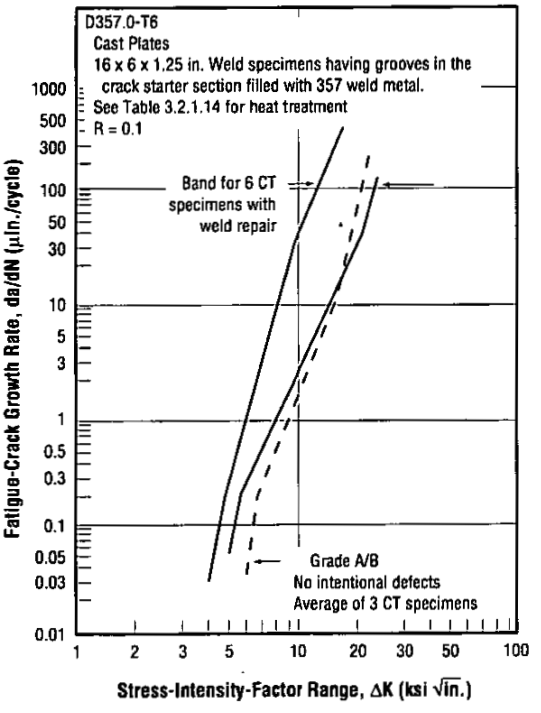

Figure 4.3.1.6 Effect of weld repair on fatigue-crack growth rates of specimens from sand-cast plates with Grade B porosity (Ref. 41)

Table 4.3.2.2 Single-shear lap bond strength of as-cast A357.0-T6 adherends with two adhesive systems (Ref. 36)

Alloy	A357.0-T6			
Form	Station 170 Bulkhead of YC-14 Fuselage			
Specimen Geometry	Flat Strips 0.12-in. Thick by 0.475-in. Wide			
Bond Surface Condition	As-received Rough Cast			
Bonding Procedure	See Table 4.3.2.3 for details			
Adhesive System (Cure Temperature)	Test Condition	Aging Condition	Single-shear Lap Bond Strength[a] (psi)	Fraction of 2024-T3 Lap Bond Strength[b]
Hysol EA 9628H (250F)	RT	Dry	5,690	0.87
		Wet[c]	5,430	0.85
	180F	Dry	4,090	0.89
		Wet	3,350	0.79
American Cyanamid FM 300 (350F)	RT	Dry	4,300	0.98
		Wet	4,730	0.99
	300F	Dry	1,660	0.65
		Wet	1,780	0.73
	350F	Dry	570	1.24
		Wet	320	0.74

[a] Average of 5 replications.

[b] ASTM D 1002 procedure; machined surfaces; same bonding; average of 5 replications.

[c] 2 weeks exposure to 100% RH at 120F.

Table 4.3.2.3 Surface preparation and bonding procedures for fabrication of lap joint test specimens (Ref. 36)

1. Solvent wipe with acetone.
2. Vapor degrease 10 minutes in trichloroethane.
3. Alkaline wash 10 minutes at 155F.[a]
4. Rinse 10 minutes in continuous flow tap water.
5. Etch 10 minutes in optimized FPL at 155F.[b]
6. Rinse 10 minutes in agitated continuous flow tap water.
7. Anodize 20 minutes in 9 - 12 percent phosphoric acid solution at 15 volts.[c]
8. Rinse 10 minutes in continuous flow tap water.
9. Dry 10 minutes with heat gun or oven at 150F.
10. Prime with American Cyanamid BR-127 approx. 0.0002 inch thick.
11. Air dry 10 minutes at RT; oven dry 60 minutes at 250F.
12. Hand-layup bond joint with binder clips for pressure.
13. Oven cure at required temperature.

[a] 1 gallon tap water, 170 gm Turco 4215, 7 ml Turco 4215 additive.

[b] 11 l tap water, 417 gm sodium dichromate, 2 l sulfuric acid, 26 gm shredded 2024-T3 Al.

[c] per ASTM D 3933; 1 l tap water, 69 ml phosphoric acid, 85 percent or 84.5 ml phosphoric acid, 75 percent.

REFERENCES

1. AMS 4241A, Aluminum Alloy Castings, Society of Automotive Engineers (July 1, 1992).
2. AMS 4249, Aluminum Alloy Castings, Society of Automotive Engineers (July 1, 1992).
3. Goehler, D.D., "Cast Aluminum Structures Technology (CAST)," AFFDL TR 77-36, Contract F33615-76-C-3111, The Boeing Co. (May 1977).
4. Goehler, D.D., "Cast Aluminum Structures Technology, Phase III (CAST)," AFFDL TR 78-7, Contract F33615-76-C-3111, The Boeing Co. (May 1978).
5. Christner R.G., and Goehler, D.D., "Cast Aluminum Structures Technology, Phase II," AFFDL TR 78-62, Contract F33615-76-C-3111, The Boeing Co. (May 1978).
6. McField, R.C., Logan, A., Faber, J.W., and Southworth, H.L., "Cast Aluminum Structures Technology (CAST) - Fabrication of Demonstration Articles and Production Hardware (Phase IV)," AFFDL TR 79-302, Contract F33615-76-C-3111, The Boeing Co. (March 1979).
7. Gunther, C.K., "Cast Aluminum Structures Technology (CAST) - Structural Test and Evaluation (Phase V) - Part II: Fatigue and Fracture Properties of Cast Aluminum Bulkheads," AFFDL TR 80-3021, Pt. II, Contract F33615-76-C-3111, The Boeing Co. (March 1979).
8. Gunther, C.K., "Cast Aluminum Structures Technology (CAST) - Structural Test and Evaluation (Phase V) - Part I: Full Scale Test," AFFDL TR 80-3021, Pt. I, Contract F33615-76-C-3111, The Boeing Co. (March 1979).
9. McLellan, D.L, "Cast Aluminum Structures Technology (CAST) - Structural Test and Evaluation (Phase V) - Part III: Static Properties Allowables," AFFDL TR 80-3021, Contract F33615-76-C-3111, The Boeing Co. (March 1979).
10. Faber, J.W., "Cast Aluminum Structures Technology (CAST) - Structural Test and Evaluation (Phase VI) - Summary Technical Report," AFFDL TR 80-3020, Contract F33615-76-C-3111, The Boeing Co. (March 1979).
11. Brondyke, K.J., and McCormick, T.F., "Melting, Remelting, Degassing/Fluxing and Handling," *Aluminum, Vol. III, Fabrication and Finishing*, K.R. Van Horn, Editor, ASM, Cleveland, OH (1967).
12. Oswalt, K.J., and Lii, Y., "Manufacturing Methods for Process Effects on Aluminum Casting Alowables," AFWAL TR 84-4117, Contract F33615-79-C-5116, Northrop Corp. (March 1985).
13. Doyle, C.E., et al., "Cast Aluminum Aircraft Structure," Vols I and II, AFWAL TR 84-4070, Contract F33615-79-C-5001, General Dynamics, Fort Worth, TX (June 1984).
14. Oswalt, K.J., and Misra, M.S., "Dendrite Arm Spacing (DAS): A Nondestructive Test to Evaluate Tensile Properties of Premium Quality Aluminum Alloy (Al-Si-Mg) Castings," *AFS International Cast Metals Journal*, Vol. 6, p. 23 (1981).
15. Tirpak, J.D., "The Variability of Fatigue-Crack Growth Life in Aluminum Casting Alloy A357-T6," AFWAL TR-86-4115 (July 1986).
16. McLellan, D.L., "Tensile Properties of A357-T6 Aluminum Castings," *Journal of Testing and Evaluation*, Vol. 8, p. 170 (July 1980).
17. Oswalt, K.J., "A Comparison of the Fatigue Behavior of High Strength Cast Aluminum Alloys 201 and A357," Northrop Corp., Aircraft Division, NOR 71-229 (December 1, 1971).
18. Alcoa Product Manual, "Premium Castings," Alcoa, Premium Castings Division, Corona, CA (1972).
19. Alcoa Premium Castings Division, Corona, CA (1969).
20. Private communication from A.F. Maloit, Pasadena, CA to W.F. Brown, Jr., Bay Village, OH.
21. Granger, D.A., Kersker, M.M., and Sawtell, R.R., "Effect of Beryllium on the Properties of A357.0 Castings," *AFS Transactions*, Vol. 92 (1984).

22. Bardes, B.P., and Flemings, M.C., "Dendrite Arm Spacing and Solidification Time in an Al-Cu Alloy," *AFS Transactions*, Vol. 74, p. 406 (1966).

23. Spear, R.E., and Gardner, G.R., "Dendrite Cell Size," *AFS Transactions*, Vol. 71, p. 209 (1963).

24. McLellan, D.L., and Tuttle, M.M., "Manufacturing Methodology Improvement for Aluminum Casting Ductility," AFWL TR-82-4135, Contract F33615-80C-3209, Boeing Military Airplane Co., (December 1982).

25. Kutchera, R.E., Schweikert, W.H., and Bailey, P.G., "Manufacturing Methods for Process Effects on Aluminum Casting Allowables," AFWAL TR 80-4176, Contract F33615-76-C-5076, General Electric Co., Aircraft Engine Business Group (June 1981).

26. Nagel, G., and Portalier, R., "Structural Modification of Aluminum-Silicon Alloys by Antimony Treatment," *AFS International Cast Metals Journal*, Vol. 5, No. 4, p. 2 (December 1980).

27. Kennerknecht, S., "Metallurgical Aspects of Quality Control in the Production of Premium Quality Aluminum Investment Casting for the Aerospace Industry," *AGARD Conference Proceedings No. 325, Advanced Castings Technology*, 54th Meeting of the AGARD Structures and Materials Panel in Brussels, Belgium (April 1982).

28. Stein, D., "Quantitative Nondestructive Tensile Testing of A356/A357 Aluminum Alloy Castings," Hughes Helicopters, Paper presented at *AFS 84th Casting Congress*, St. Louis, MO (April 1980).

29. Faber, J.W., "Metallographic Analysis Techniques Used During the Cast Aluminum Structures Technology (CAST) Program," *12th National SAMPE Technical Conference*, p. 768 (October 1980).

30. Development: Premium Alloy Castings of Alloy A357.0-T6, Alcoa, Pittsburgh, PA (1971).

31. Gunther, C.K., "Cast Aluminum Primary Aircraft Structure," Boeing Military Aircraft Co., p. 323 (December 1979).

32. Tirpak, J.D., "Elevated Temperature Properties of Cast Aluminum Alloys A201-T7 and A357-T6," AFWAL TR-85-4114 (November 1985).

33. SAE ARP 1947, "Dendrite Arm Spacing of Structural Aircraft Quality D357 Aluminum Alloy Castings, Determination and Acceptance of" (October 1, 1985).

34. "Standards for Aluminum Sand and Permanent Mold Castings," The Aluminum Association, Washington, D.C.

35. Tan, Y.-H., Lee, S.-L., and Lin, Y.-L., "Effects of Beryllium and Iron Content on Plane-Strain Fracture Toughness in A357 Alloys," *Metallurgical and Materials Trans. A*, Vol. 26A, pp. 2937-2945 (November 1995).

36. Kuhbander, R.J., Caldwell, S.J., and Fiscus, S.E., "Cast Aluminum Bonding Study," AFWAL TR-88-4065 (May 1988).

37. Bosworth, T.J., "Repair Welding Aluminum Castings, Part 2," *Modern Casting*, Vol. 74:4, pp. 19-22 (April 1984).

38. Anon., "Alcotec Alloy R-A357.0 Al-Si-Mg-Be Filler Wire for Sand and Permanent Mold Castings," *Alloy Digest* (September 1992).

39. Marsh, L.E., and Reinemann, G., "Premium Quality Aluminum Castings Theory, Practice, and Assurances," *Transactions of the American Foundrymen's Society*, Vol. 87, pp. 413-422 (1979).

40. Zinkham, R.E., "A New Quality Assurance Tool for Aluminum Castings, Including A Study of A357 Fracture Toughness," *Transactions of the American Foundryman's Society*, Vol. 97, pp. 959-968 (May 1989).

41. Ozelton, M.W., Mocarski, S.J., and Porter, P.G., "Durability and Damage Tolerance of Aluminum Castings," WL-TR-91-4111, Contract F33615-85-C-5015, Northrop Corp. (October 1991).

42. Srivatsan, T.S., Meyers, C.W., and Berry, J., "A Method for Determining the Tensile Properties and Anisotropy of Aluminum Alloys," *Journal of Testing and Evaluation*, Vol. 15:4, pp. 196-204 (July 1987).

43. AMS 4241A, Aluminum Alloy Castings, Society of Automotive Engineers (July 1, 1992).

44. AMS 4245B, Aluminum Alloy Welding Wire, Society of Automotive Engineers (July 1996).

45. Military Specification MIL-A-21180D, Aluminum Alloy Castings - High Strength Amendment 1 (December 14, 1991).

46. ASTM B 108 Aluminum Alloy Permanent Mold Castings, ASTM Annual Book of Standards, Vol. 02.02 (1995).

47. ASTM B 108 Aluminum Alloy Castings - High Strength, ASTM Annual Book of Standards, Vol. 02.02 (1995).